

Production of Heavy neutrino in next-to-leading order QCD at the LHC and beyond

Arindam Das,^{a,1} Partha Konar,^b Swapan Majhi^c

^a*Department of Physics and Astronomy, University of Alabama, Tuscaloosa, Alabama, 35487, USA*

^b*Theoretical Physics Group, Physical Research Laboratory, Ahmedabad-380009, India*

^c*Department of Physics, Achhruram Memorial College, Purulia, WB, 723202, India*

E-mail: adas8@ua.edu, konar@prl.res.in, majhi.majhi@gmail.com

ABSTRACT: Majorana and pseudo-Dirac heavy neutrinos are introduced into the type-I and inverse seesaw models, respectively, in explaining the naturally small neutrino mass. TeV scale heavy neutrinos can also be accommodated to have a sizable mixing with the Standard Model light neutrinos, through which they can be produced and detected at the high energy colliders. In this paper we consider the Next-to-Leading Order QCD corrections to the heavy neutrino production, and study the scale variation in cross-sections as well as the kinematic distributions with different final states at 14 TeV LHC and also in the context of 100 TeV hadron collider. The repertoire of the Majorana neutrino is realized through the characteristic signature of the same-sign dilepton pair, whereas, due to a small lepton number violation, the pseudo-Dirac heavy neutrino can manifest the trileptons associated with missing energy in the final state. Using the $\sqrt{s} = 8$ TeV, 20.3 fb^{-1} and 19.7 fb^{-1} data at the ATLAS and CMS respectively, we obtain prospective scale dependent upper bounds of the light-heavy neutrino mixing angles for the Majorana heavy neutrinos at the 14 TeV LHC and 100 TeV collider. Further exploiting a recent study on the anomalous multilepton search by CMS at $\sqrt{s} = 8$ TeV with 19.5 fb^{-1} data, we also obtain the prospective scale dependent upper bounds on the mixing angles for the pseudo-Dirac neutrinos. We thus project a scale dependent prospective reach using the NLO processes at the 14 TeV LHC.

¹Corresponding author.

Contents

1	Introduction	1
2	Neutrino Mass Mechanism	3
3	Heavy neutrino production at the high energy colliders	5
4	Scale dependent kinematic distributions in trilepton channel	10
5	Scale dependent prospective upper bound on the mixing angles	15
5.1	Same sign dilepton plus two jet production signal	15
5.2	Trilepton associated with missing transverse energy signal	19
6	Conclusion	22

1 Introduction

The journey of Large Hadron Collider (LHC) in its 7 and 8 TeV run has been extremely successful in discovering, and further constraining the properties of long-awaited Higgs boson [1, 2] of Standard Model (SM). However, LHC is still lacking any clinching signature yet from the beyond the Standard Model (BSM) physics. With general wisdom, there exists a broad agreement in admitting the SM as, at most a very accurate description for low energy effective theory of particle physics. This notion is embolden from the fact, that the SM falls short to explain divers outstanding issues both in theory and in explaining some crucial experimental observations.

The most recent observations on the neutrino oscillation phenomena [3–8] have established that tiny neutrino mass and the flavor mixing of the SM neutrinos which is one of the divers mysteries in SM. The existence of such a tiny neutrino mass requires us to extend the SM. The seesaw mechanism [9–15] is probably the simplest idea to extend the SM, which can explain the small neutrino mass naturally. The SM-singlet heavy right-handed Majorana neutrinos induce the dimension five operators [16] leading to very small light Majorana neutrino masses. If such heavy neutrino mass lies in the electroweak scale, then the heavy neutrinos can be produced in the high energy colliders [17–57] from various initial states. The heavy neutrinos are singlet under the SM gauge group therefore they can be coupled to the SM gauge bosons through the mixing with the light SM neutrinos vis Dirac Yukawa coupling. The Dirac Yukawa coupling can be sizable for the electroweak scale heavy neutrinos in

general Casas-Ibarra parameterization [58], while reproducing the neutrino oscillation data.

There is another kind of seesaw mechanism, commonly known as inverse seesaw [59, 60], where the tiny Majorana mass is generated from the small lepton number violating parameters, rather than being suppressed by the heavy neutrino mass in conventional seesaw mechanism. In case of inverse seesaw the heavy neutrinos are pseudo-Dirac and the Dirac Yukawa coupling could be of order one, satisfying the neutrino oscillation data. Thus at the high energy colliders the pseudo-Dirac heavy neutrinos can be produced through the sizable mixing with the SM neutrinos. In our analysis we choose the LHC at the center of mass energy $\sqrt{s} = 14$ TeV and a proposed proton-proton collider at the center of mass energy $\sqrt{s} = 100$ TeV [61] which can enlighten the new physics era including the heavy neutrino physics more precisely with its higher fact finding ability.

Apart from these seesaw mechanisms there are different other simple ways which can also be tested in colliders. Type-II seesaw where the SM is extended by an SU(2) triplet scalar, see [62–74] for detailed studies. The other one is the type-III seesaw which is obtained by the extension of the SM with an SU(2) triplet fermion, see [75–82] for detailed studies, (see [83] for the NLO analysis in type-III seesaw). Additional interesting possibility of generate naturally small neutrino mass is from higher-dimensional operators at the TeV scale and thus testable at the collider [84–86].

The heavy neutrino can be produced at the high energy colliders from various initial states among them the leading contributions come from the processes generated from the quark-quark ($q\bar{q}'$), quark-gluon (qg) and gluon-gluon (gg) initial states. Among these processes the $q\bar{q}'$ initial state is the commonly studied leading order (LO) production channel for the heavy neutrinos, where as, the other channels can contribute in its Next-to-Leading-Order (NLO) and Next-to-Next-to-Leading-Order (NNLO) QCD corrections together with the corresponding LO processes. In this paper we concentrate on the QCD NLO production processes including the virtual correction contributions and the real emission processes. For the LO processes we demonstrate the production of the heavy neutrino for different factorization (μ_F) scales associated to the parton density functions (PDFs) considering the 14 TeV LHC and in the context of proposed 100 TeV hadron collider. On the other hand, NLO processes are studied with different choices of factorization (μ_F) as well as renormalization (μ_R) scales juxtaposing together with LO contributions.

The paper is organized in the following way. In Sec. 2 we introduce the type-I seesaw and inverse seesaw models. These are the primary models we concentrate in our present analysis. In Sec. 3 we calculate the production cross-section of the heavy neutrino at the high energy colliders. We discuss the methodology followed with different choice of parameters in estimating in leading order and next-to-leading order production of heavy neutrinos. We also opened up discussion on the scale

variation related to these production cross-sections. In Sec. 4 we study the scale dependent kinematic distributions of different kinematic measurable quantities in the heavy neutrino production from the trilepton plus missing energy final state. In Sec. 5 we utilize the current Large Hadron Collider (LHC) data from ATLAS and CMS to put scale dependent upper bounds on the mixing angles between the light-heavy neutrinos. Sec. 6 is dedicated to the conclusion.

2 Neutrino Mass Mechanism

In type-I seesaw [9–15], we introduce SM gauge-singlet right handed Majorana neutrinos N_R^β , where β is the flavor index. N_R^β couple with SM lepton doublets ℓ_L^α and the SM Higgs doublet H . The relevant part of the Lagrangian is

$$\mathcal{L} \supset -Y_D^{\alpha\beta} \bar{\ell}_L^\alpha H N_R^\beta - \frac{1}{2} m_N^{\alpha\beta} \overline{N_R^{\alpha C}} N_R^\beta + H.c.. \quad (2.1)$$

After the spontaneous electroweak symmetry breaking by the vacuum expectation value (VEV), $H = \begin{pmatrix} \frac{v}{\sqrt{2}} \\ 0 \end{pmatrix}$, we obtain the Dirac mass matrix as $M_D = \frac{Y_D v}{\sqrt{2}}$. Using the Dirac and Majorana mass matrices we can write the neutrino mass matrix as

$$M_\nu = \begin{pmatrix} 0 & M_D \\ M_D^T & m_N \end{pmatrix}. \quad (2.2)$$

Diagonalizing this matrix we obtain the seesaw formula for the light Majorana neutrinos as

$$m_\nu \simeq -M_D m_N^{-1} M_D^T. \quad (2.3)$$

For $m_N \sim 100$ GeV, one may find that the extremely minuscule $Y_D \sim 10^{-6}$ is needed to construct some light neutrino mass of order $m_\nu \sim 0.1$ eV. However, using the general parameterization based on Casas-Ibarra [58], one gets the Yukawa coupling expressed in terms of a orthogonal matrix which remains completely arbitrary and hence can be large. Following this mechanism Y_D can be phenomenologically viable, as large as order one, and this is the case we consider in our present work.

There is another seesaw mechanism, so-called inverse seesaw [59, 60], where the light Majorana neutrino mass is generated through tiny lepton number violation. The relevant part of the Lagrangian is given by

$$\mathcal{L} \supset -Y_D^{\alpha\beta} \bar{\ell}_L^\alpha H N_R^\beta - m_N^{\alpha\beta} \overline{S_L^\alpha} N_R^\beta - \frac{1}{2} \mu_{\alpha\beta} \overline{S_L^\alpha} S_L^{\beta C} + H.c., \quad (2.4)$$

where N_R^α and S_L^β are two SM-singlet heavy neutrinos with the same lepton numbers, m_N is the Dirac mass matrix, and μ is a small Majorana mass matrix violating the

lepton numbers. After the electroweak symmetry breaking we obtain the neutrino mass matrix as

$$M_\nu = \begin{pmatrix} 0 & M_D & 0 \\ M_D^T & 0 & m_N^T \\ 0 & m_N & \mu \end{pmatrix}. \quad (2.5)$$

Diagonalizing this mass matrix we obtain the light neutrino mass matrix

$$M_\nu \simeq M_D m_N^{-1} \mu m_N^{-1T} M_D^T. \quad (2.6)$$

Note that the smallness of the light neutrino mass originates from the small lepton number violating term μ . The smallness of μ allows the $m_D m_N^{-1}$ parameter to be order one even for an electroweak scale heavy neutrino. Since the scale of μ is much smaller than the scale of m_N , the heavy neutrinos become the pseudo-Dirac particles. This is the main difference between the type-I and the inverse seesaws.

Through the seesaw mechanism, a flavor eigenstate (ν) of the SM neutrino is expressed in terms of the mass eigenstates of the light (ν_m) and heavy (N_m) Majorana neutrinos such as

$$\nu \simeq \nu_m + V_{\ell N} N_m, \quad (2.7)$$

where $V_{\ell N}$ is the mixing between the SM neutrino and the SM-singlet heavy neutrino, and we have assumed a small mixing, $|V_{\ell N}| \ll 1$. Using the mass eigenstates, the charged current interaction for the heavy neutrino is given by

$$\mathcal{L}_{CC} \supset -\frac{g}{\sqrt{2}} W_\mu \bar{\ell} \gamma^\mu P_L V_{\ell N} N_m + h.c., \quad (2.8)$$

where ℓ denotes the three generations of the charged leptons in the vector form, and $P_L = \frac{1}{2}(1 - \gamma_5)$ is the projection operator. Similarly, the neutral current interaction is given by

$$\mathcal{L}_{NC} \supset -\frac{g}{2c_w} Z_\mu [\bar{N}_m \gamma^\mu P_L |V_{\ell N}|^2 N_m + \{\bar{\nu}_m \gamma^\mu P_L V_{\ell N} N_m + h.c.\}], \quad (2.9)$$

where $c_w = \cos \theta_w$ with θ_w being the weak mixing angle. The main decay modes of the heavy neutrino are $N \rightarrow \ell W$, $\nu_\ell Z$, $\nu_\ell h$. The corresponding partial decay widths are respectively given by

$$\begin{aligned} \Gamma(N \rightarrow \ell W) &= \frac{g^2 |V_{\ell N}|^2 (m_N^2 - m_W^2)^2 (m_N^2 + 2m_W^2)}{64\pi m_N^3 m_W^2}, \\ \Gamma(N \rightarrow \nu_\ell Z) &= \frac{g^2 |V_{\ell N}|^2 (m_N^2 - m_Z^2)^2 (m_N^2 + 2m_Z^2)}{128\pi c_w^2 m_N^3 m_Z^2}, \\ \Gamma(N \rightarrow \nu_\ell h) &= \frac{|V_{\ell N}|^2 (m_N^2 - m_h^2)^2}{32\pi m_N} \left(\frac{1}{v}\right)^2. \end{aligned} \quad (2.10)$$

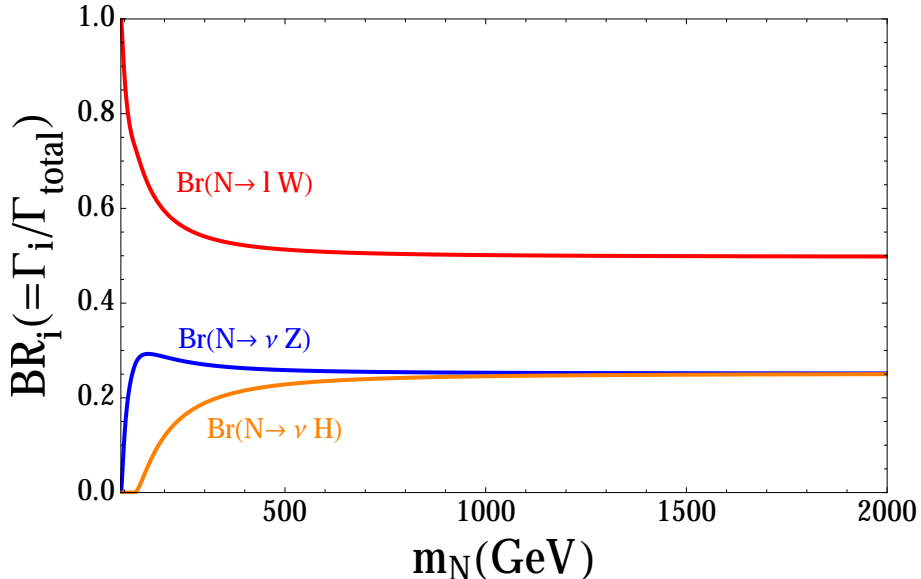


Figure 1. Heavy neutrino branching ratios (BR_i) for different decay modes are shown with respect to the heavy neutrino mass (m_N).

The decay width of heavy neutrino into charged gauge bosons being twice as large as neutral one owing to the two degrees of freedom (W^\pm). We plot the branching ratios $BR_i (= \Gamma_i / \Gamma_{\text{total}})$ of the respective decay modes (Γ_i) with respect to the total decay width (Γ_{total}) of the heavy neutrino into W , Z and Higgs bosons in Fig. 1 as a function of the heavy neutrino mass (m_N). Note that for larger values of m_N , the branching ratios can be obtained as

$$BR(N \rightarrow \ell W) : BR(N \rightarrow \nu Z) : BR(N \rightarrow \nu H) \simeq 2 : 1 : 1. \quad (2.11)$$

3 Heavy neutrino production at the high energy colliders

We implement our model in the event generator `MadGraph5-aMC@NLO` [87–89] and calculate the production cross-section of the heavy neutrino at the LO and NLO respectively. The full automation of NLO computation is based on two main steps. The code for the evaluation of one loop is made through `MADLOOP`[90] and the born and real-emission amplitudes have been computed through `MadFKS`[91] together with the integration and matching scheme of `MC@NLO`. `MadLoop` evaluate one loop amplitude by using Ossola-Papadopoulos-Pittau `OPP`[92] integrand-reduction technique which is implemented in `CutTools`[93]. In `MadFKS`, subtraction method have been used by `FKS`[94] formalism. The showering and hadronization of the events were performed with `PYTHIA6.4` for LO and `PYTHIA6Q` for the NLO processes [95] bundled

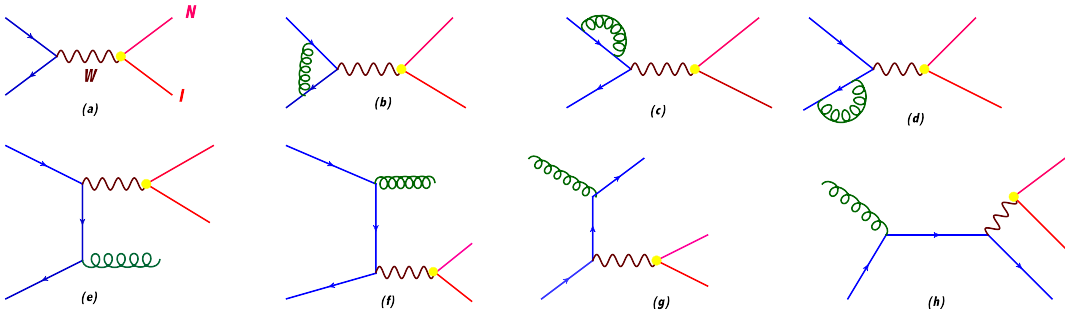


Figure 2. Representative Feynman diagrams for the leading order $N\ell$ production from the $q\bar{q}$ process at hadron collider at the Born process or LO(a). Corresponding NLO diagrams including Virtual Corrections(b – d) and Real Emissions(e – h) contributing from different initial states are shown in rest of the diagrams.

in MadGraph with anti- k_T algorithm. The hadronic jets are clustered with anti- k_T formalism using FastJet[96]¹.

The hadronic cross-sections have been calculated by convoluting LO (NLO) parton distribution functions (PDF), namely, CTEQ6L1 (CTEQ6M) with LO (NLO) partonic cross-section which has been done through MadGraph5-aMC@NLO. We choose $\alpha_s(m_Z) = 0.130$ in CTEQ6L1 for LO and $\alpha_s(M_Z) = 0.1180$ in CTEQ6M for NLO according to [99], $m_Z = 91.188$ GeV, $m_W = 80.423$ GeV and $G_F = 1.166 \times 10^{-5}$ GeV⁻² as electroweak input parameters. Thereof, $\alpha_{QED} = 1/132.54$ and $\sin^2 \theta_W = 0.22217$ are computed via LO electroweak relations. In this analysis we have considered two types of final states. One of them is $N\ell$ from the W boson mediated process. In Fig. 2 the leading Feynman diagrams including the Born level in Fig. 2(a), virtual diagrams in Fig. 2(b – d) and real emissions diagrams in Fig. 2(e – h) initiated from quark-antiquark or quark-gluon are demonstrated. The other final state we considered is the $N\nu$ from the Z boson mediated process which we can extract easily from Fig. 2. We have computed the LO cross-sections for the fixed mass with the variation of factorisation scale (μ_F). Since the LO cross-section depends only on the μ_F through LO PDFs and we varied as

$$\mu_F = \xi m_N \tag{3.1}$$

where ξ is the scale factor varying between 0.1 to 10. Whereas the NLO cross-section

¹In our final drafting phase Ref. [56] appeared with the NLO prediction of the heavy neutrino production using MadGraphMC@NLO which overlaps with a part our result consistently depending upon the choices of scale and selection cuts. It is important to mention that we have used our independently developed code for the type-I and Inverse seesaw mechanisms in MadGraphMC@NLO, fixing bugs with the active support from the MadGraph team [97] and finally with private communications. The implementation of scale variations were suggested in [98], although we finally used the straightforward method bypassing the SyaCalc.

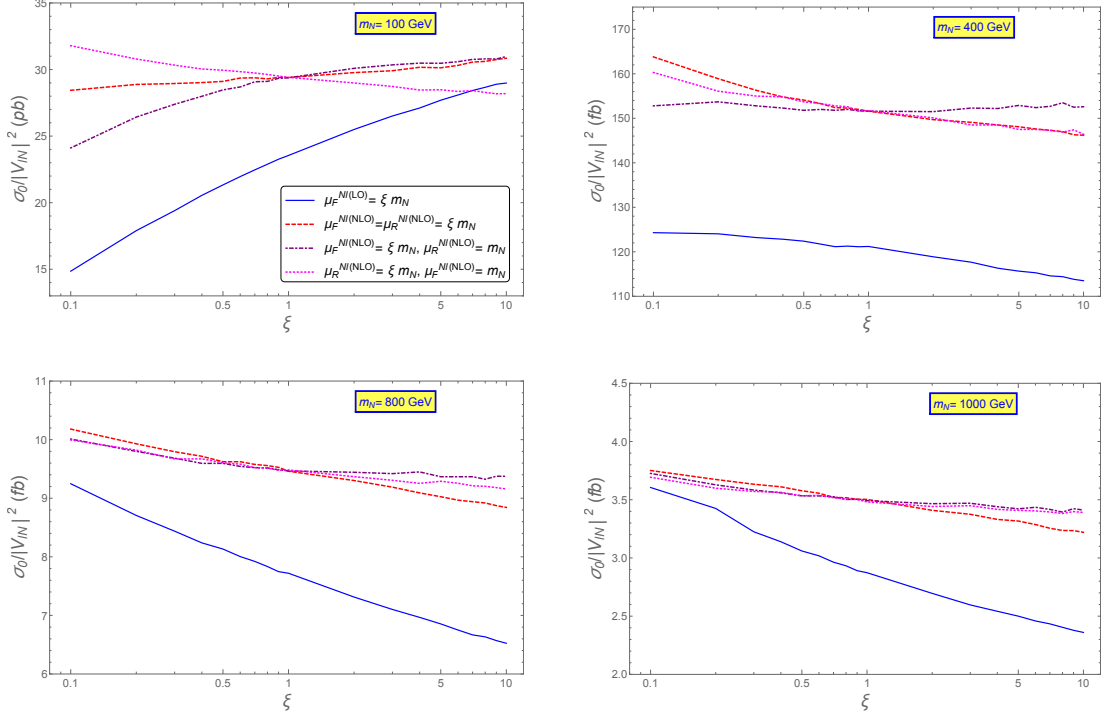


Figure 3. Scale variation of the heavy neutrino production process $pp \rightarrow \ell N$ at the 14 TeV LHC comparing the LO with the NLO estimates at different scale choices. Plots are shown for four different heavy neutrino mass m_N . Cross-sections are shown as normalized with the value of $|V_{\ell N}|^2$.

depends on both the scale, namely, the factorization scale (μ_F) through PDFs and the renormalisation scale (μ_R) through NLO partonic cross-section (mainly due to the couplings renormalisation). For simplicity, throughout the present analysis we have considered to vary both these scales as,

$$\mu_F = \mu_R = \xi m_N \quad \text{with} \quad 0.1 \leq \xi \leq 10. \quad (3.2)$$

We have produced the scale dependent cross-sections normalized by the square of the mixing angle $|V_{\ell N}|^2$ for a fixed choice of heavy neutrino mass m_N at 100 GeV, 400 GeV, 800 GeV and 1 TeV at the 14 TeV LHC for the LO and NLO processes with varying ξ between 0.1 to 10. This scale dependence are shown in Fig. 3. In the same plot, we also display the theoretical scale uncertainty in NLO calculation due to μ_F alone by fixing the renormalisation scale at the corresponding heavy neutrino mass ($\mu_R = m_N$). Since later dependence only enters at the the NLO level in the form of $\alpha_s(\mu_R)$, one expects the μ_F scale dependence which actually soften in NLO calculation. The other scenario by fixing the factorization scale at the corresponding heavy neutrino mass ($\mu_F = m_N$) is also shown by changing only the μ_R scale in the same plot. For $m_N = 100$ GeV, the leading order cross-section σ_{LO} varies sharply and in-

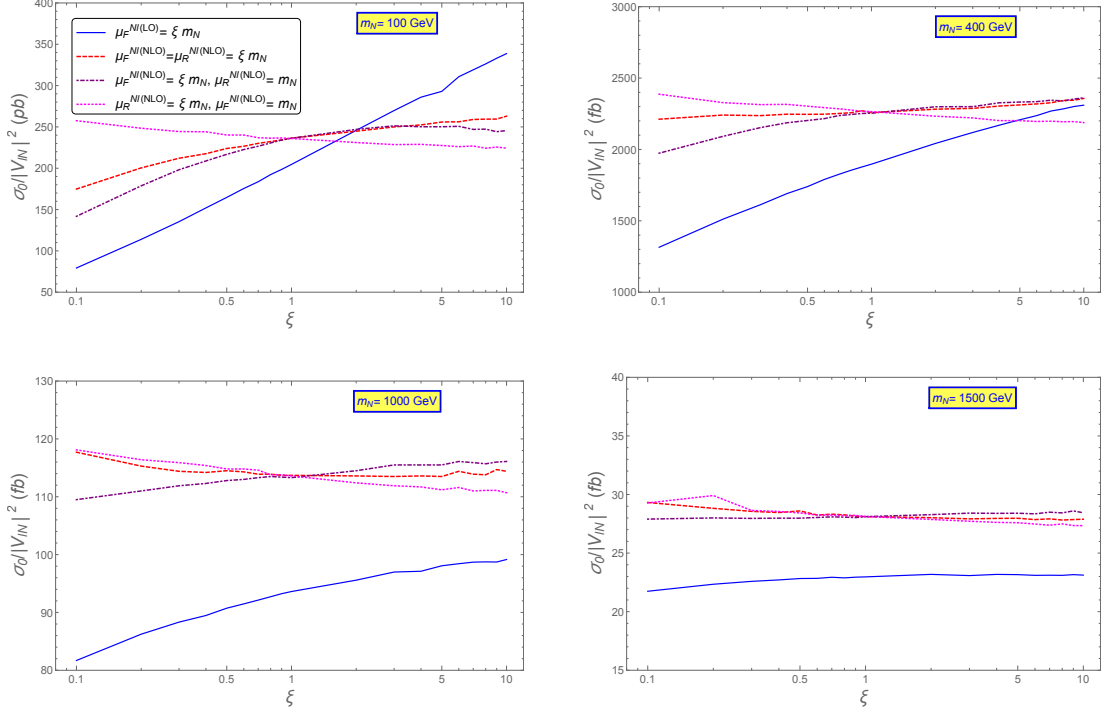


Figure 4. Scale variation of the heavy neutrino production process $pp \rightarrow \ell N$ at the 100 TeV HC comparing the LO with the NLO estimates at different scale choices. Plots are shown for four different heavy neutrino mass m_N . Cross-sections are shown as normalized with the value of $|V_{\ell N}|^2$.

creasing almost monotonically by a factor of two approximately with increase in scale factor (ξ), which indicates a substantial amount of theoretical uncertainty present in the LO result. This is because of only the LO quark-antiquark flux with varying scale factor ξ^2 . Whereas in NLO, it is three fold - the scale dependent logarithmic terms present in partonic cross-sections, the NLO PDF fluxes (namely, quark-antiquark, quark-gluon and antiquark-gluon) as well as strong coupling constant and hence the strong scale dependent part cancels among themselves. Therefore this strong scale dependence has been softened by including the NLO calculation which varies slowly with the scale. At the larger choices of heavy neutrino mass, both the LO and the NLO cross sections decrease with ξ variation, although the basic feature of softening of NLO variations are evident in all such examples.

The scale dependent results for 100 TeV collider considering m_N at 100 GeV, 400 GeV, 1 TeV and 1.5 TeV are also shown in Fig. 4. Here the scale variation of the leading order cross-section varies rather sharply especially for lower value of m_N , which provides the LO cross-section dominating over the NLO prediction for $\xi > 2$. This steep rising of LO cross-section is mainly due to the LO PDF (CTEQ6L1) sets. On the other hand the NLO cross-sections reduce this PDF scale uncertainty

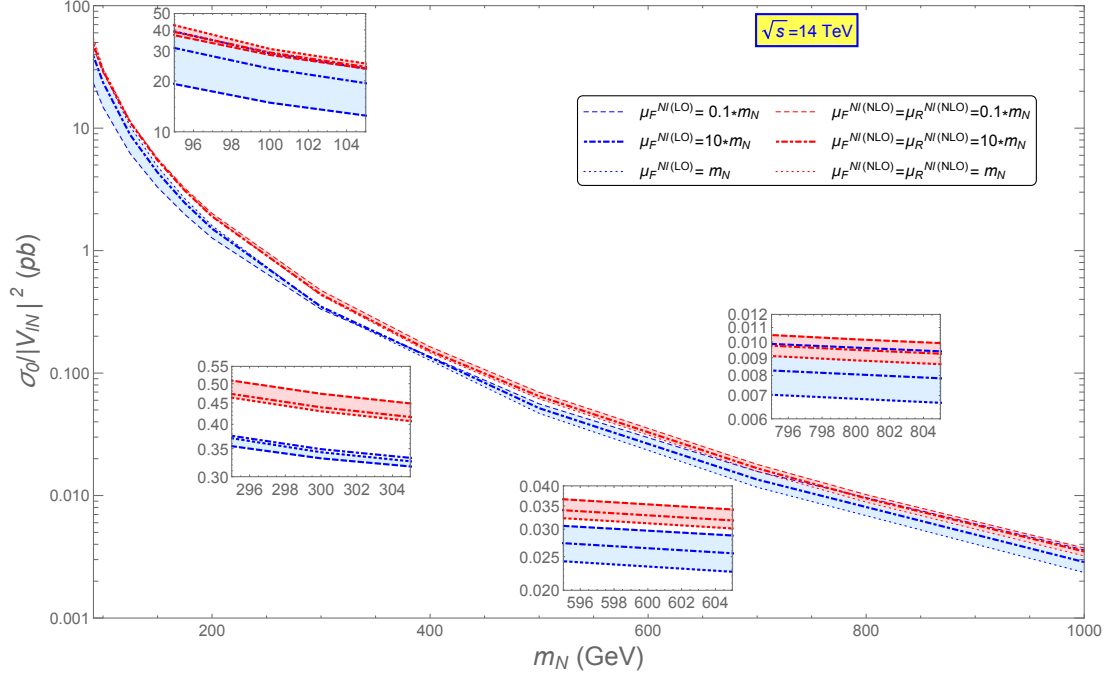


Figure 5. Heavy neutrino production cross-section from $pp \rightarrow \ell N$ at the 14 TeV LHC as a function of m_N . Both LO and NLO predictions are shown with the scale variation effect as a band. The cross-sections are normalized by the square of the mixing angles. Inset plots showing with zoomed bands at different masses.

significantly so that the NLO cross-section remains almost flat with respect to ξ for all m_N at the 100 TeV hadron collider.

The scale variations of the heavy neutrino production cross-sections, normalized by the square of the mixing matrix, is further demonstrated as a function of m_N at 14 TeV LHC and 100 TeV hadron collider in Fig. 5 and Fig. 6. In these figures, the blue (red) bands shows the scale dependence of the σ_{LO} (σ_{NLO}). It is clear from these figures that the strong scale dependence reduces significantly at NLO cross-section as compared to LO one.

We also study the next-to-leading order predictions for $N\nu$ final state mediated by the Z boson. The scale dependent cross-sections at 14 TeV LHC and 100 TeV hadron collider are given in Fig. 7. We consider the heavy neutrino mass at 100 GeV and 800 GeV. We used the same scale dependence for the $N\nu$ final state as we did in $N\ell$ final state for LO and NLO respectively. At 14 TeV the LO cross-section at $m_N = 100$ GeV increases with ξ at a faster rate than the NLO process whereas for $m_N = 800$ GeV the LO cross-section decreases with the increase in ξ with a faster rate than that in NLO. On the other hand at 100 TeV collider the LO process at $m_N = 100$ GeV takes over the NLO for $\xi > 1.9$. For $m_N = 800$ GeV the LO cross-section increases with the increase in ξ but the NLO cross-section remains more or less same for $\xi > 0.5$. Following our earlier demonstration on $N\ell$, we have also shown

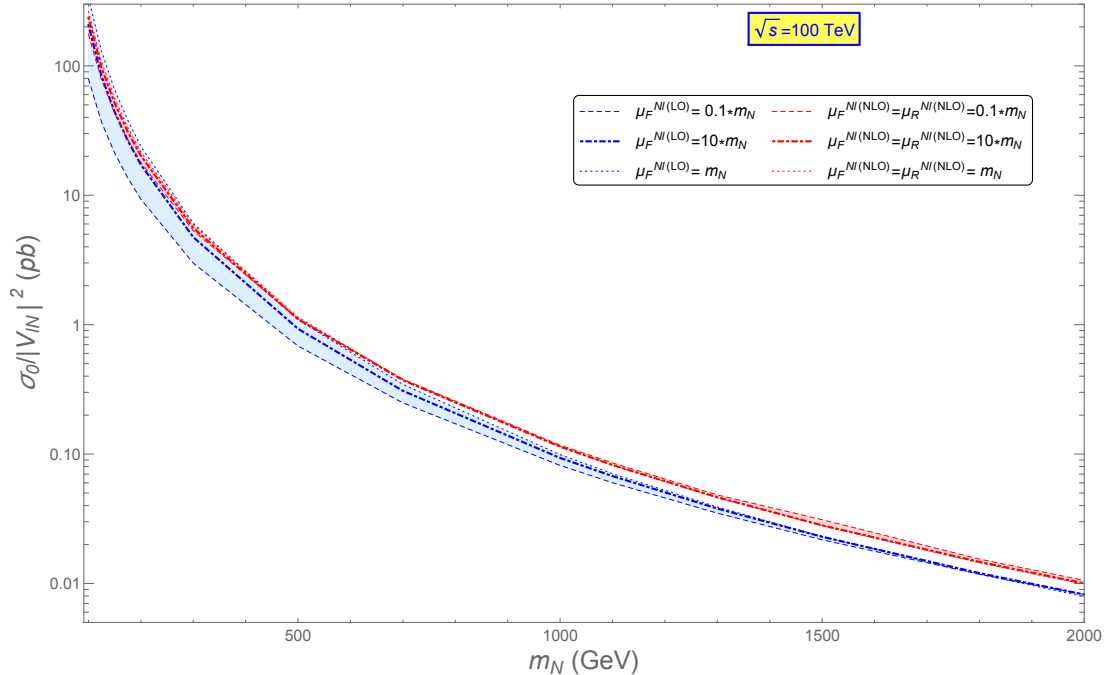


Figure 6. Heavy neutrino production cross-section from $pp \rightarrow \ell N$ at the 100 TeV hadron collider as a function of m_N . Both LO and NLO predictions are shown with the scale variation effect as a band.

in Fig. 8 the cross-sections for the $N\nu$ final state as a function of m_N at 14 TeV LHC and 100 TeV collider along with the corresponding scale dependence bands.

4 Scale dependent kinematic distributions in trilepton channel

In this section we consider the pseudo-Dirac heavy neutrino production at the hadron collider and study its decay process for the 14 TeV LHC and 100 TeV collider. For further demonstration we choose the heavy neutrino with mass $m_N = 400$ GeV. Different kinematic distributions are constructed both for the LO and NLO calculations by choosing both the factorization scale as well as renormalisation scale varying simultaneously (as in Eq.3.2) with a scale factor ξ between 0.1 and 10. The pseudo-Dirac heavy neutrino is involved in the inverse seesaw mechanism to generate the neutrino mass. The collider phenomenology of inverse seesaw mechanism has been studied in [22–24, 26] for the LO process with trilepton final state for a fixed scale. In case of inverse seesaw mechanism the Yukawa coupling could be high enough to enhance the heavy neutrino production. However, due to the small lepton number violating parameter² the heavy neutrino becomes pseudo-Dirac. In this analysis we

²See, [22] for the detailed discussion about the smallness of the lepton number violating parameter in case of inverse seesaw mechanism.

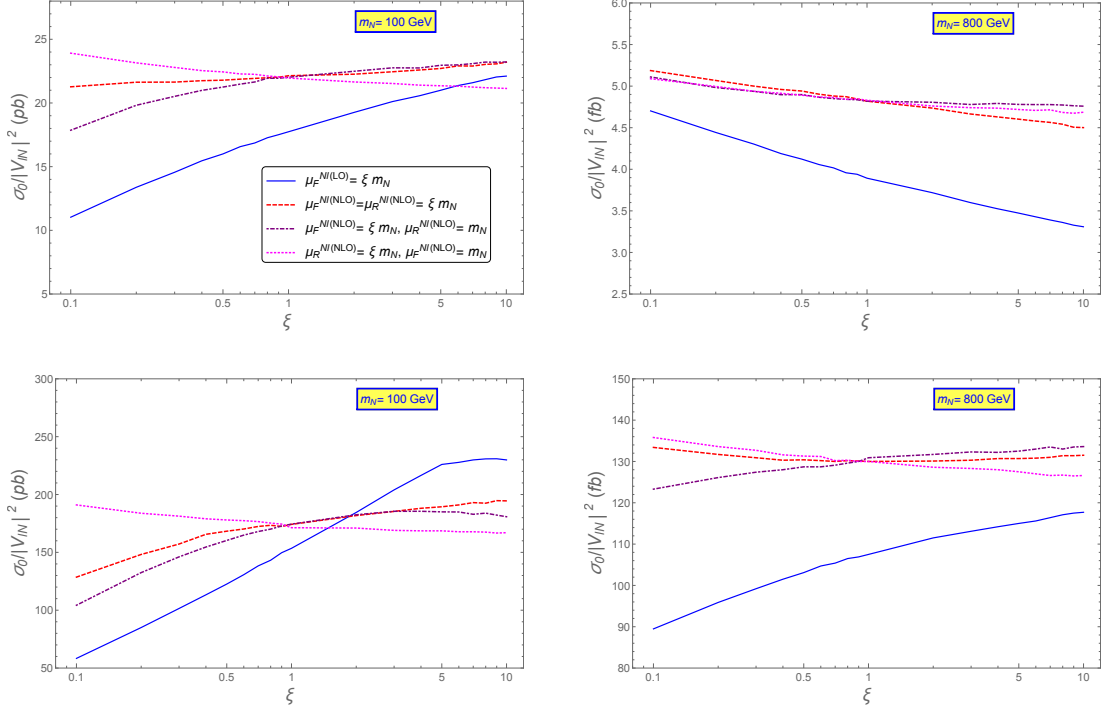


Figure 7. Scale variation of the heavy neutrino production process $pp \rightarrow \nu N$ at the (upper) 14 TeV LHC (lower) 100 TeV hadron collider comparing the LO with the NLO estimates at different scale choices. Plots are shown for two different heavy neutrino mass m_N . Cross-sections are shown as normalized with the value of $|V_{eN}|^2$.

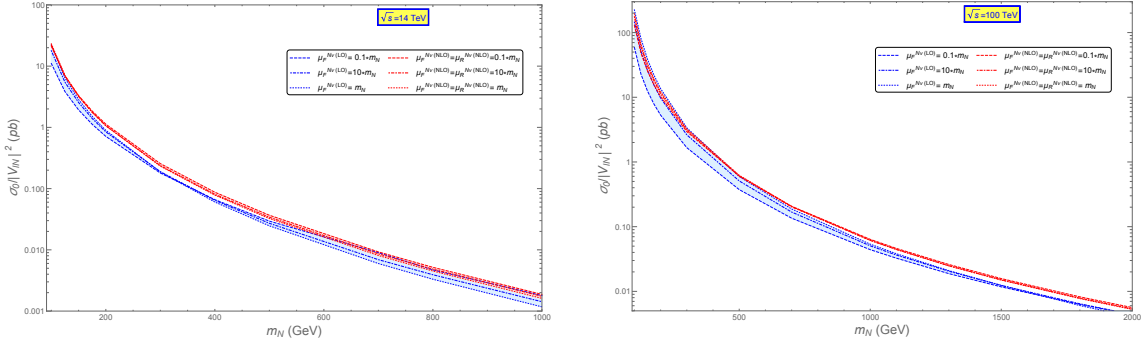


Figure 8. Heavy neutrino production cross-section normalized by the square of the mixing angle from $pp \rightarrow \nu N$ at the 14 TeV LHC as a function of m_N at the 14 TeV (Left panel) and 100 TeV (right panel). Both LO and NLO predictions are shown with the scale variation effect as a band.

consider the Single Flavor (SF) scenario, where only one heavy neutrino is light and accessible to the high energy colliders. It couples with one generation of the lepton flavor. For simplicity, we consider that the heavy neutrino is coupled with the second

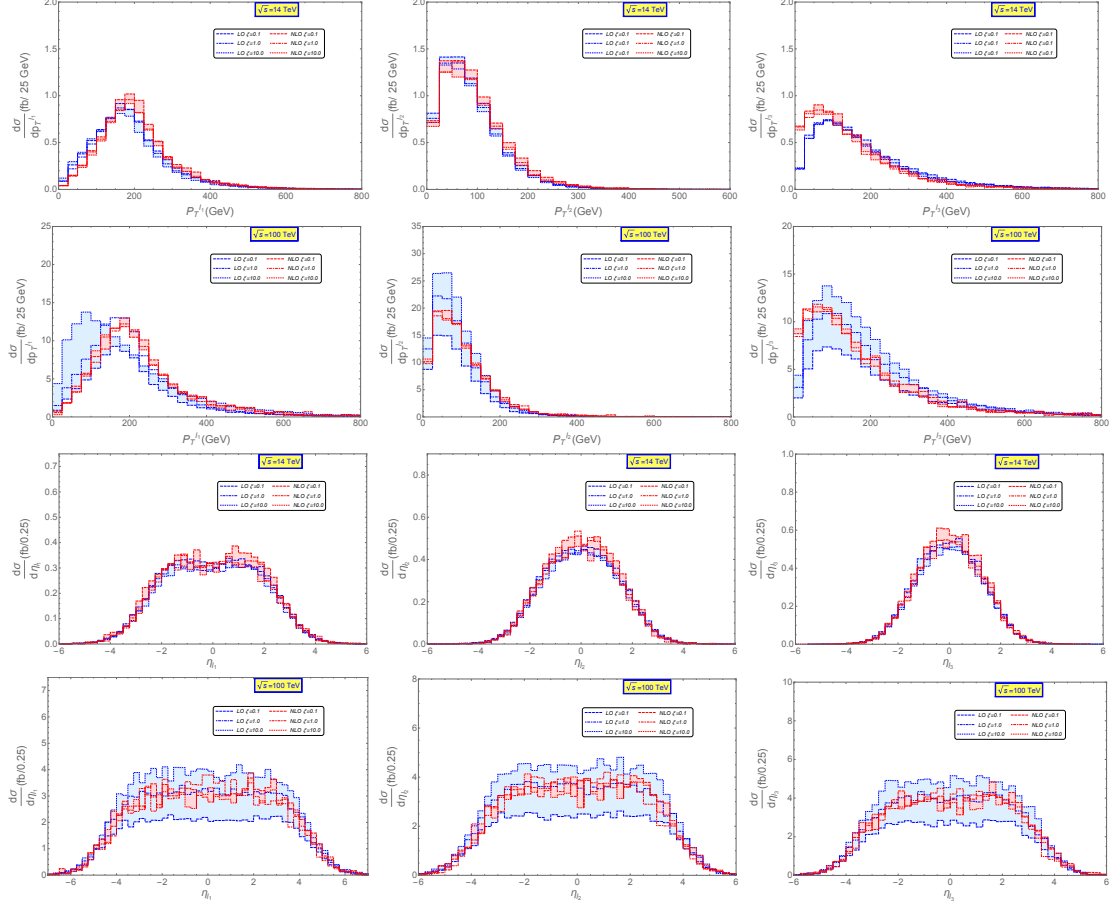


Figure 9. Scale variation of the differential scattering cross-section as a function of the transverse momentum of leptons ($p_T^{\ell_i}$, $i = 1, 2, 3$) and pseudorapidity of leptons (η^{ℓ_i} , $i = 1, 2, 3$) in case of trilepton production channel for $m_N = 400$ GeV. The first row corresponds to the $p_T^{\ell_i}$ distributions at $\sqrt{s} = 14$ TeV LHC whereas the second row represents the same at $\sqrt{s} = 100$ TeV collider. The third row corresponds to the η^{ℓ_i} distributions at $\sqrt{s} = 14$ TeV LHC whereas the fourth row represents the same at the $\sqrt{s} = 100$ TeV collider. The differential scattering cross-section distributions are normalized by $|V_{\ell N}|^2$.

generation of the lepton flavor³. As a result the golden channel for the final state signal is the trilepton plus missing energy which is given by

$$\begin{aligned}
 pp &\rightarrow \ell_1^+ N, N \rightarrow \ell_2^- W^+, W^+ \rightarrow \ell_3^+ \nu_{\ell_3} \\
 pp &\rightarrow \ell_1^- \bar{N}, \bar{N} \rightarrow \ell_2^+ W^-, W^- \rightarrow \ell_3^- \bar{\nu}_{\ell_3}.
 \end{aligned}
 \tag{4.1}$$

Within the same set of the model parameters as described in the last section, we show the differential distributions of scattering cross-section as a function of the

³Another possibility could be possible where we can introduce two generations of the degenerate heavy neutrinos and each generation couples with the single, corresponding lepton flavor which we can name as Flavor Diagonal(FD) case. See, [23, 24] for the study on FD case.

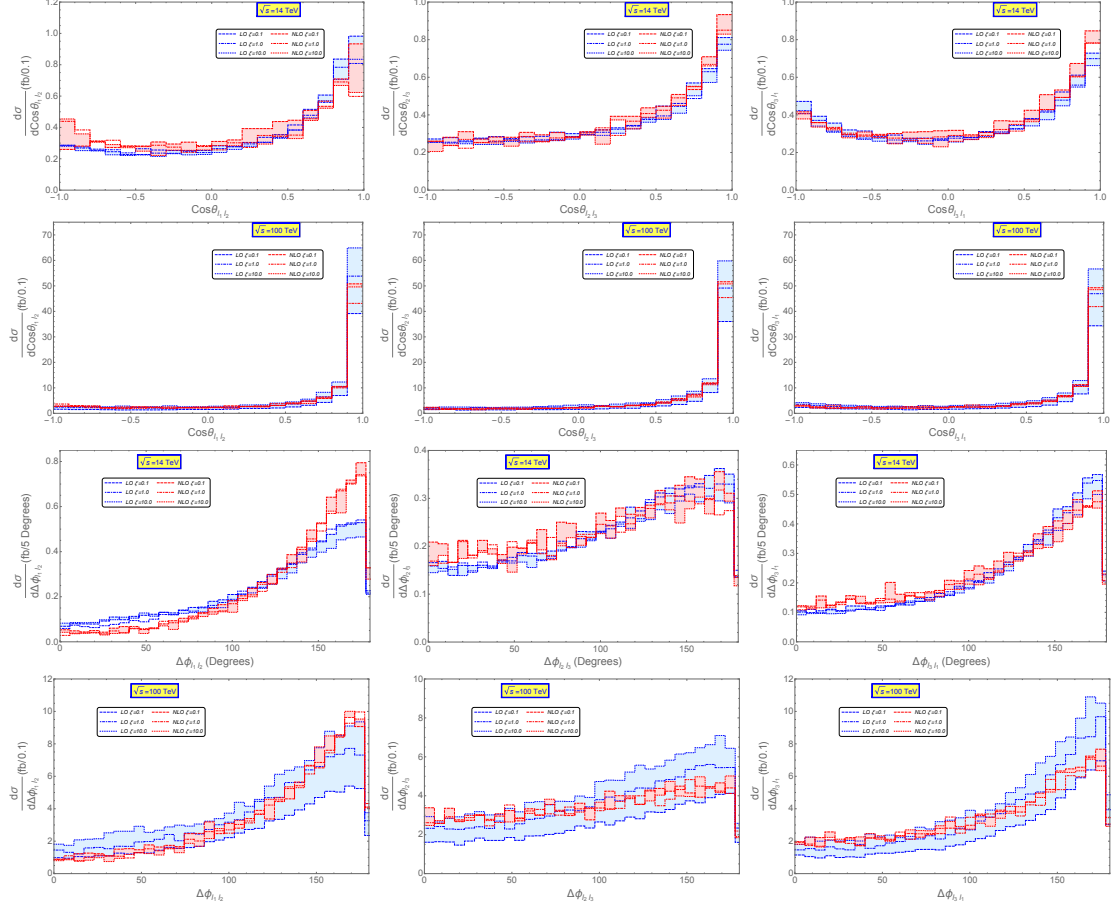


Figure 10. Scale variation of the differential scattering cross-section distribution with respect to $\cos\theta_{\ell_i\ell_j}$ of the leptons with $i = 1, 2, 3, j = 1, 2, 3$ and $i \neq j$ and $\Delta\phi_{\ell_i\ell_j}$ of the leptons with $i = 1, 2, 3, j = 1, 2, 3$ and $i \neq j$ for the tripleton production channel for $m_N = 400$ GeV. The first row corresponds to $\cos\theta_{\ell_i\ell_j}$ at $\sqrt{s} = 14$ TeV LHC whereas the second row represents the $\sqrt{s} = 100$ TeV collider. The third row corresponds to $\Delta\phi_{\ell_i\ell_j}$ at $\sqrt{s} = 14$ TeV LHC whereas the fourth row represents the same at $\sqrt{s} = 100$ TeV collider. The differential cross-section distributions are normalized by $|V_{\ell N}|^2$.

transverse momenta for these three leptons separately, $p_T^{\ell_i}$ for $i = 1, 2, 3$ in Fig. 9 for the 14 TeV LHC and 100 TeV collider. In case of 14 TeV, the NLO distributions dominate over the LO distributions in the high transverse momentum region for ℓ_1 and ℓ_2 . Whereas for ℓ_3 , the NLO distributions dominate over the LO distributions quite impressively in the low transverse momentum region. This behavior is due to inclusion of extra radiation at the NLO process as well as showering effect. In the 100 TeV case, similar situations are demonstrated, however leading order scale uncertainties are exceptionally large, again due to LO PDF sets as mentioned earlier.

We exhibit the pseudo-rapidity distributions in Fig. 9. The $\eta^{\ell_{2,3}}$ distributions at the 14 TeV are sharper than that of η^{ℓ_1} , resulting the production of these two

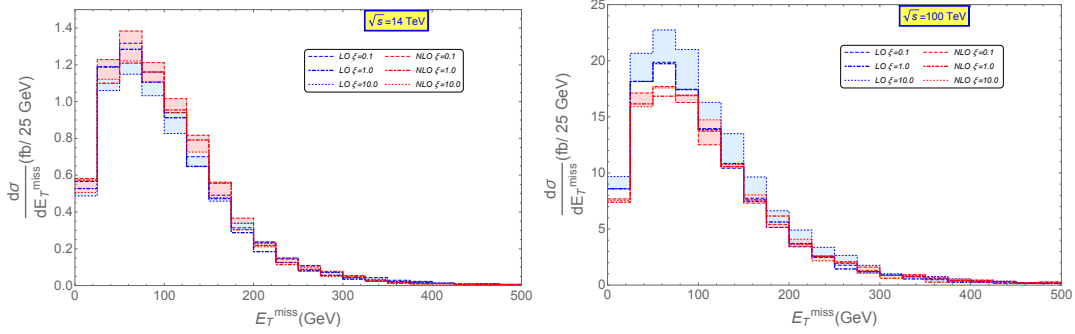


Figure 11. Scale variation of the differential scattering cross-section as a function of the missing transverse momentum (η^{ℓ_i} , $i = 1, 2, 3$) in case of trilepton production channel for $m_N = 400$ GeV. The left panel corresponds to case at $\sqrt{s} = 14$ TeV LHC whereas the right panel represents the $\sqrt{s} = 100$ TeV collider. The differential cross-section distributions are normalized by $|V_{\ell N}|^2$.

leptons in the central region. The scale variations for the LO and NLO cases are not very high in the 14 TeV LHC. In comparison to that, the scale variations at the LO is very prominent in the 100 TeV case. The scale variation for the NLO calculation soften strikingly as expected.

To study the different dilepton correlating observables in terms of LO and NLO calculation with their corresponding scale uncertainties, in Fig. 10 we display the differential distributions for scattering cross-section with respect to the angles between the leptons, $\cos \theta_{\ell_i \ell_j}$ for $i = 1, 2, 3$, $j = 1, 2, 3$ and $i \neq j$. The production of the leptons with large polar angular separation is abundant, although tend to choose smaller one since main production channel involves the contributions from both the valence and sea quarks. This effect is quite more evident at 100 TeV machine, where the leptons are mostly produced at small polar angle. The difference between the azimuthal angle between the two leptons, namely, $\Delta \phi_{\ell_i \ell_j}$ of the leptons with $i = 1, 2, 3$, $j = 1, 2, 3$ and $i \neq j$ are also shown in Fig. 10. One notice that both the $\Delta \phi_{\ell_1 \ell_2}$ and $\Delta \phi_{\ell_1 \ell_3}$ distributions show some enhancement when leptons are produced back to back, supported by the leptons produced in boosted heavy neutrino decay. This peak is further enhanced in the NLO calculation. However, $\Delta \phi_{\ell_1 \ell_2}$ remains flat in both calculations. Scale uncertainty is also shown to be substantially controlled in NLO estimates.

The scale dependent differential scattering cross-section as a function of missing transverse energy, E_T^{miss} , are given Fig. 11 where the LO and NLO variations have good agreements at 14 TeV LHC. NLO distribution enhances at larger E_T^{miss} . We can make the same observation at the NLO and LO cases for the 100 TeV collider.

5 Scale dependent prospective upper bound on the mixing angles

In this section, we study the prospective upper bounds on the mixing angles between the heavy neutrino and the SM light neutrinos. We consider two different scenarios such as type-I seesaw which involves a heavy Majorana neutrino and inverse seesaw which introduces a pseudo-Dirac heavy neutrino. Due to the large lepton number violation, the type-I seesaw scenario is observed through the characteristic same sign dilepton plus dijet final state. On the other hand due to a very small lepton number violating parameter, optimal observable being the trilepton plus missing energy signal for inverse seesaw case. Using these mechanisms and existing searches done by LHC at $\sqrt{s} = 8$ TeV (Run-1) we obtain prospective search reaches at the LHC at $\sqrt{s} = 14$ TeV (Run-2) and proposed proton-proton collider at $\sqrt{s} = 100$ TeV.

5.1 Same sign dilepton plus two jet production signal

For simplicity we consider the case that only one generation of the Majorana heavy neutrino is lighter enough and accessible to the LHC which couples to only the second generation of the lepton flavor. To generate the events in the **MadGraph** we use the **CTEQ6L1** for the LO and **CTEQ6M** for the NLO ($\mu_F = \mu_R$) cases respectively. We study the scale dependent same sign dilepton plus dijet signal cross-section as a function of the heavy neutrino mass (m_N). The signal cross-section at the level of LO and NLO are calculated as $\sigma(\xi)_{LO}$ and $\sigma(\xi)_{NLO}$ respectively for the same sign dimuon production,

$$pp \rightarrow N\mu^\pm \rightarrow \mu^\pm\mu^\pm jj. \quad (5.1)$$

Thus corresponding values are expressed the 14 TeV LHC ($\sigma(\xi)_{LO}^{14}, \sigma(\xi)_{NLO}^{14}$) and 100 TeV collider ($\sigma(\xi)_{LO}^{100}, \sigma(\xi)_{NLO}^{100}$). Comparing our generated events with the recent ATLAS results [100] at the 8 TeV LHC with the luminosity 20.3 fb^{-1} , we obtain an upper limit on the mixing angles between the Majorana type heavy neutrino and the SM leptons as a function of m_N for $\xi = 0.1, 1.0, 10.0$. In the ATLAS analysis the upper bound of the production cross-section (σ^{ATLAS}) is obtained for the final state with the same sign di-muon plus dijet as a function of m_N . Using these 14 TeV leading order (LO) scale dependent cross-sections, we obtain the prospective upper bounds on the mixing angles for different values of $\xi = \xi'$ which is chosen to be either of $= \{0.1, 1, 10\}$,

$$|V_{\ell N}|^2(\xi')_{LO}^{14} \lesssim \frac{\sigma^{ATLAS}}{\sigma(\xi')_{LO}^{14}}, \quad (5.2)$$

whereas those for the NLO case at the 14 TeV are given as

$$|V_{\ell N}|^2(\xi')_{NLO}^{14} \lesssim \frac{\sigma^{ATLAS}}{\sigma(\xi')_{NLO}^{14}}, \quad (5.3)$$

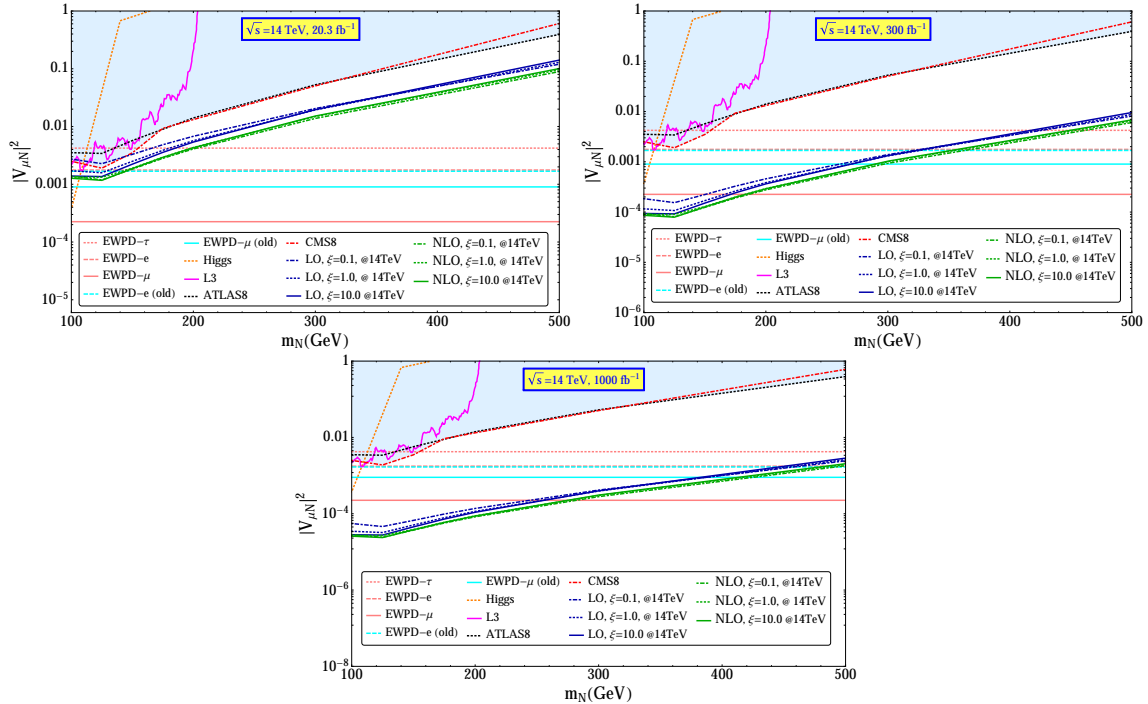


Figure 12. Figure shows the prospective upper bounds of square on the mixing angles as a function of m_N using the ATLAS data at the 8 TeV [100] at 20.3 fb^{-1} luminosity for the same sign dilepton plus dijet case. The scale dependent LO and NLO prospective upper bounds at the 14 TeV LHC at 20.3 fb^{-1} luminosity (left panel, upper row), at 300 fb^{-1} luminosity (right panel, upper row) and 1000 fb^{-1} (lower row) are given. These bounds are compared to (i) the χ^2 -fit to the LHC Higgs data [101] (Higgs), (ii) from a direct search at LEP [102](L3), valid only for the electron flavor, (iv) CMS limits from $\sqrt{s} = 8$ TeV LHC data [103] (CMS8) and ATLAS [100] (ATLAS8), for a heavy Majorana neutrino of the muon flavor and (v) indirect limits from the global fit to the electroweak precision data (EWPD) from [104–106] for electron (cyan, EWPD-e(old)) and muon (cyan, EWPD- μ (old)) flavors(new values can be found from [107]), for tau (dotted, EWPD- τ) electron (solid, EWPD- e) and muon (dashed, EWPD- μ) flavors). The shaded region is excluded by the 8 TeV data.

At the 100 TeV we use Eqs. (5.2) and (5.3) replacing the cross-sections at the 14 TeV LHC with those at the 100 TeV collider. The calculated prospective upper bounds on the mixing angles are shown in Fig. 12 along with the bounds from ATLAS [100], CMS [103], LEP (L3) [102], electroweak precision data for tau (EWPD- τ), electron (EWPD-e) and muon (EWPD- μ) [108, 109] (see, [104–106] for previous analysis), and finally LHC Higgs data (Higgs) [101] (see, [107, 110, 111] for some updated analysis). Comparing our results with the 8 TeV results given by ATLAS [100] we give a prospective upper bound on the mixing angle at 14 TeV LHC with 20.3 fb^{-1} luminosity for different values of $\xi = 0.1, 1.0, 10.0$ at the LO and NLO.

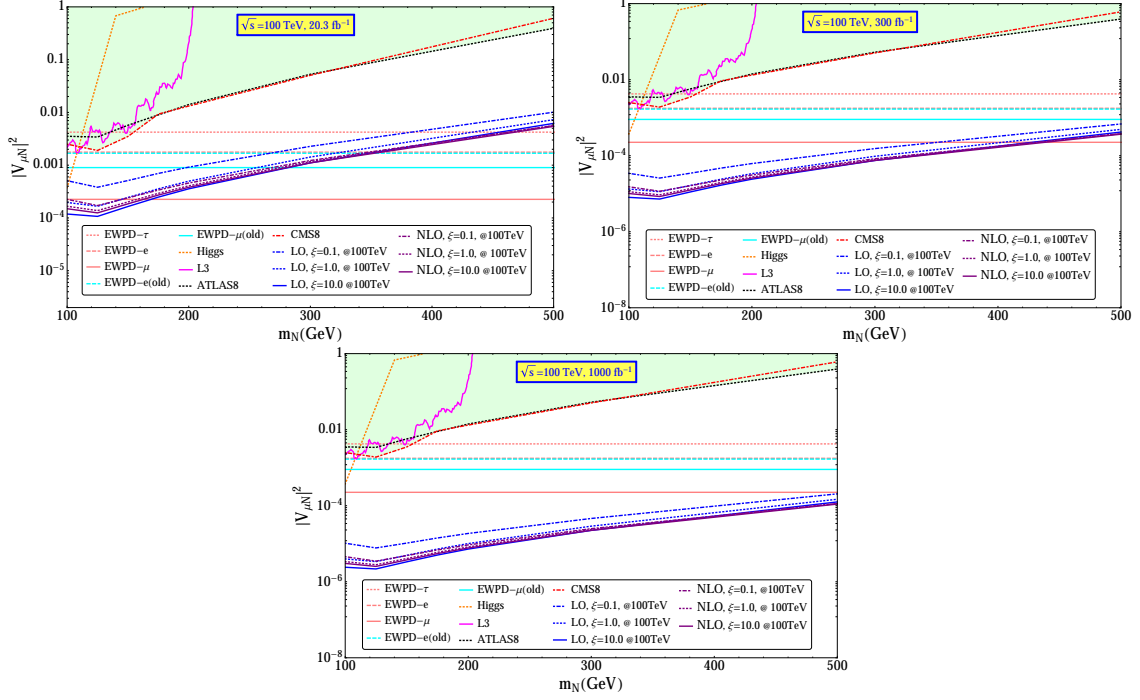


Figure 13. Figure shows the prospective upper bounds of square on the mixing angles as a function of m_N using the ATLAS data at the 8 TeV [100] at 20.3 fb^{-1} luminosity for the same sign dilepton plus dijet case. The scale dependent LO and NLO prospective upper bounds at the 100 TeV LHC at 20.3 fb^{-1} luminosity (left panel, upper row), at 300 fb^{-1} luminosity (right panel, upper row) and 1000 fb^{-1} (lower row) are given. These bounds are compared to (i) the χ^2 -fit to the LHC Higgs data [101] (Higgs), (ii) from a direct search at LEP [102](L3), valid only for the electron flavor, (iv) CMS limits from $\sqrt{s} = 8 \text{ TeV}$ LHC data [103] (CMS8) and ATLAS [100] (ATLAS8), for a heavy Majorana neutrino of the muon flavor and (v) indirect limits from the global fit to the electroweak precision data (EWPD) from [104–106] for electron (cyan, EWPD-e(old)) and muon (cyan, EWPD- μ (old)) flavors(new values can be found from [107] , for tau (dotted, EWPD- τ) electron (solid, EWPD- e) and muon (dashed, EWPD- μ) flavors). The shaded region is excluded by the 8 TeV data.

We notice that the scale dependence at LO is very clear for $m_N \lesssim 300 \text{ GeV}$ in comparison to the NLO case at the 14 TeV LHC. The LO and NLO results could be comparable to the EWPD at the 14 TeV. Which we can easily verify using the LHC results in Run–2 at the 14 TeV. We have also studied the prospective upper bounds on the mixing angles at the 100 TeV collider for the LO and NLO cases at 20.3 fb^{-1} luminosity. We have noticed that for $m_N \lesssim 250 \text{ GeV}$, the mixing angle could be a factor better than those given by EWPD. An improved prospective search reach by an order of magnitude (more) for 300 fb^{-1} (1000 fb^{-1}) luminosity is also given in Fig. 12 for the 14 TeV LHC. We have also calculated a prospective search reach for

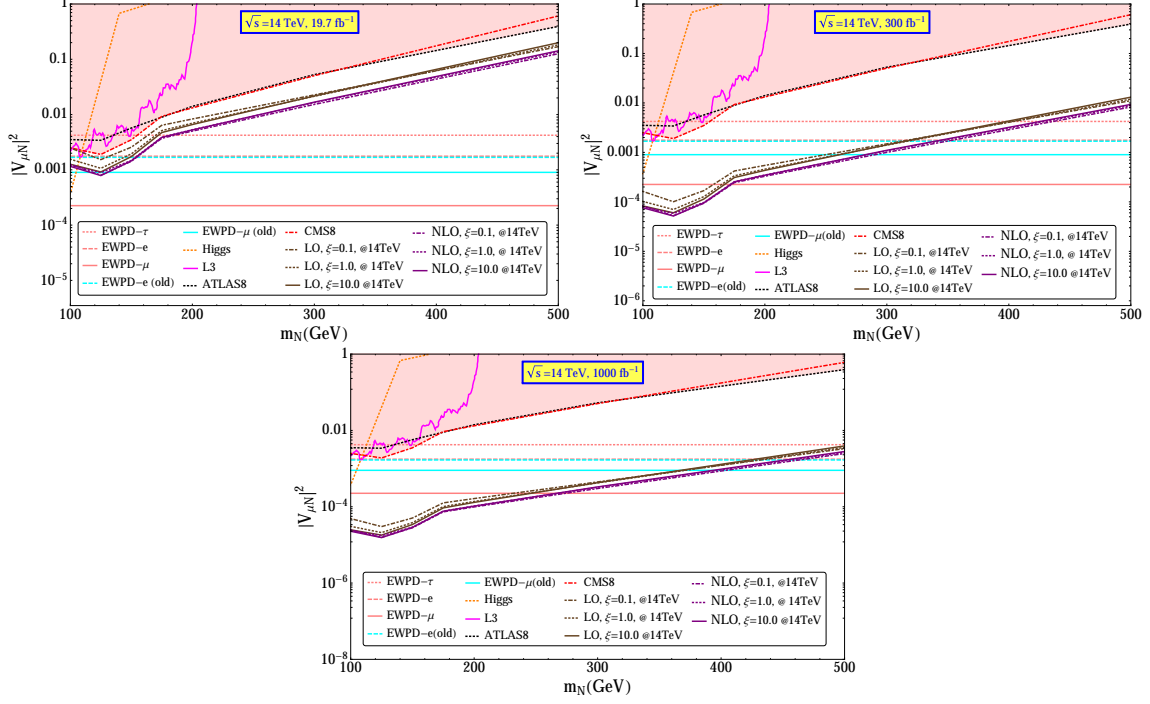


Figure 14. Figure shows the upper bounds on square of the mixing angles as a function of m_N using the CMS data at the 8 TeV [103] at 19.7 fb^{-1} luminosity for the same sign dilepton plus dijet case. The scale dependent LO and NLO prospective upper bounds at the 14 TeV LHC at 20.3 fb^{-1} luminosity (left panel, upper row), at 300 fb^{-1} luminosity (right panel, upper row) and 1000 fb^{-1} (lower row) are given. The bounds are compared to (i) the χ^2 -fit to the LHC Higgs data [101] (Higgs), (ii) from a direct search at LEP [102](L3), valid only for the electron flavor, (iv) ATLAS limits from $\sqrt{s} = 8 \text{ TeV}$ LHC data [100] (ATLAS 8) and CMS [103], for a heavy Majorana neutrino of the muon flavor and (v) indirect limits from the global fit to the electroweak precision data (EWPΔ) from [104–106] for electron (cyan, EWPΔ-e(old)) and muon (cyan, EWPΔ- μ (old)) flavors(new values can be found from [107]), for tau (dotted, EWPΔ- τ) electron (solid, EWPΔ- e) and muon (dashed, EWPΔ- μ) flavors). The shaded region is excluded by the 8 TeV data.

the 100 TeV Collider at 20.3 fb^{-1} , 300 fb^{-1} and 1000 fb^{-1} luminosities in Fig. 13. The improvement in search reach of the mixing angle from a factor to an order of magnitude with respect to the EWPΔ can be obtained at the 100 TeV.

Recently the CMS has performed the same-sign dilepton plus dijet search [103]. Using this result and adopting the same procedure for the ATLAS result we calculate the prospective upper bound on the mixing angles at the 14 TeV LHC for the LO and NLO cases at 19.7 fb^{-1} . The results are shown in Fig. 13. A clear scale dependence is observed for $m_N \lesssim 300 \text{ GeV}$ for the LO case whereas the mixing angle around 120 GeV is comparable to the EWPΔ. The scale dependence is not very high in the NLO case in comparison to the LO case. We can easily verify using the LHC

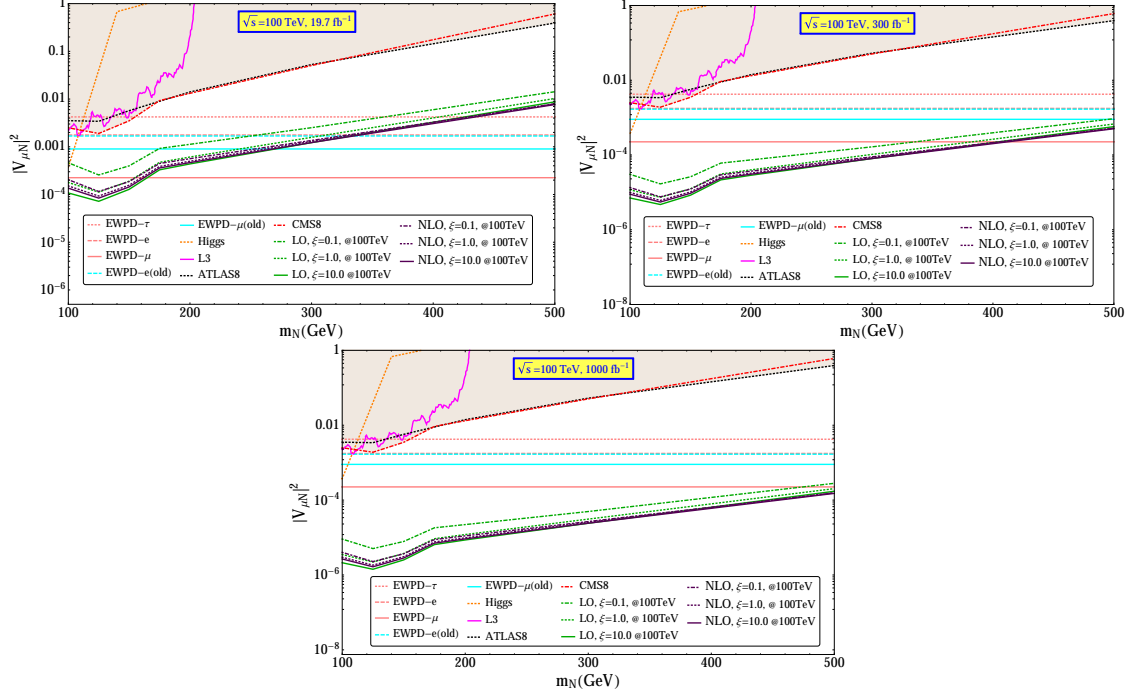


Figure 15. Figure shows the upper bounds on square of the mixing angles as a function of m_N using the CMS data at the 8 TeV [103] at 19.7 fb^{-1} luminosity for the same sign dilepton plus dijet case. The scale dependent LO and NLO prospective upper bounds at the 100 TeV LHC at 20.3 fb^{-1} luminosity (left panel, upper row), at 300 fb^{-1} luminosity (right panel, upper row) and 1000 fb^{-1} (lower row) are given. The bounds are compared to (i) the χ^2 -fit to the LHC Higgs data [101] (Higgs), (ii) from a direct search at LEP [102](L3), valid only for the electron flavor, (iv) ATLAS limits from $\sqrt{s} = 8 \text{ TeV}$ LHC data [100] (ATLAS 8) and CMS [103], for a heavy Majorana neutrino of the muon flavor and (v) indirect limits from the global fit to the electroweak precision data (EWPD) from [104–106] for electron (cyan, EWPD-e(old)) and muon (cyan, EWPD- μ (old)) flavors(new values can be found from [107]), for tau (dotted, EWPD- τ) electron (solid, EWPD- e) and muon (dashed, EWPD- μ) flavors). The shaded region is excluded by the 8 TeV data.

results in Run–2 at the 14 TeV. An improved prospective search reach by an order of magnitude (more) for 300 fb^{-1} (1000 fb^{-1}) luminosity is also given in Fig. 14 for the 14 TeV LHC. We have also depicted the prospective search reach in Fig. 15 for the 100 TeV Collider at 19.7 fb^{-1} , 300 fb^{-1} and 1000 fb^{-1} luminosities where we can improve the upper bound on the mixing angle from a factor up to an order of magnitude with respect to the EWPD from low to high luminosities.

5.2 Tripleton associated with missing transverse energy signal

We consider two cases in this analysis. One is the Flavor Diagonal case (FD), where we employ three generations of the degenerate heavy neutrinos and each generation

couples with the single, corresponding lepton flavor. The other one is the Single Flavor case (SF) where only one of the heavy neutrinos is accessible to the LHC and having mass in the Electroweak scale being coupled to only the first or second generation of the lepton flavor. In this analysis we use the CTEQ6M PDF [112] for generating the NLO($\mu_F = \mu_R$) processes to compute the scale dependent trilepton plus missing energy events with $\xi = 0.1, 1.0$ and 10.0 at $\sqrt{s} = 14$ TeV LHC using MadGraph-aMC@NLO bundled with PYTHIA6Q using anti- k_T algorithm for jet clustering in FastJet. We use the hadronized events in Delphes [113] to produce events after the detector simulation. The trilepton plus missing energy mode is given in Eq. 4.1. After the detector simulation we have considered the events with $3\ell + E_T^{miss} + n$ -jets where $n = 0, 1$ and 2 .

Recently the CMS has studied the anomalous multilepton plus missing energy final state at the 8 TeV [114]. We adopt their search result for our trilepton analysis and compare our trilepton plus missing energy final state after the detector simulation to put a prospective upper limit on the mixing angle at the 14 TeV. The cuts we used for this analysis according to [114] are itemized below:

- (i) The transverse momentum of each lepton: $p_T^\ell > 10$ GeV.
- (ii) The transverse momentum of at least one lepton: $p_T^{\ell, \text{leading}} > 20$ GeV.
- (iii) The jet transverse momentum: $p_T^j > 30$ GeV.
- (iv) The pseudo-rapidity of leptons: $|\eta^\ell| < 2.4$ and of jets: $|\eta^j| < 2.5$.
- (v) The lepton-lepton separation: $\Delta R_{\ell\ell} > 0.1$ and the lepton-jet separation: $\Delta R_{\ell j} > 0.3$.
- (vi) The invariant mass of each OSSF (opposite-sign same flavor) lepton pair: $m_{\ell^+\ell^-} < 75$ GeV or > 105 GeV to avoid the on- Z region which was excluded from the CMS search. Events with $m_{\ell^+\ell^-} < 12$ GeV are rejected to eliminate background from low-mass Drell-Yan processes and hadronic decays.
- (vii) The scalar sum of the jet transverse momenta: $H_T > 200$ GeV.
- (viii) The missing transverse energy: $50 \text{ GeV} < E_T^{miss} < 100$ GeV.

To derive the limits on $|V_{\ell N}|^2$, we calculate the signal cross-section normalized by the square of the mixing angle as a function of the heavy neutrino mass m_N for both SF and FD cases, by imposing the CMS selection criteria listed above for different scale values of ξ at the NLO process.⁴ Passing the generated detector events through all the

⁴It should be mentioned clearly that omitting the Z -pole we are excluding the effects of the other trilepton channels like $pp \rightarrow N\ell$, $N \rightarrow Z\nu$ followed by $Z \rightarrow \ell^+\ell^-$ [49, 50] exclusively from the present analysis. There is another channel $pp \rightarrow N\bar{N}$ which will be suppressed by $|V_{\ell N}|^4$ compared to the W mediated channels in Fig. 2. However, see [115–122] for some recent analyses on $N\bar{N}$ production from the B–L model due to its rich phenomenology.

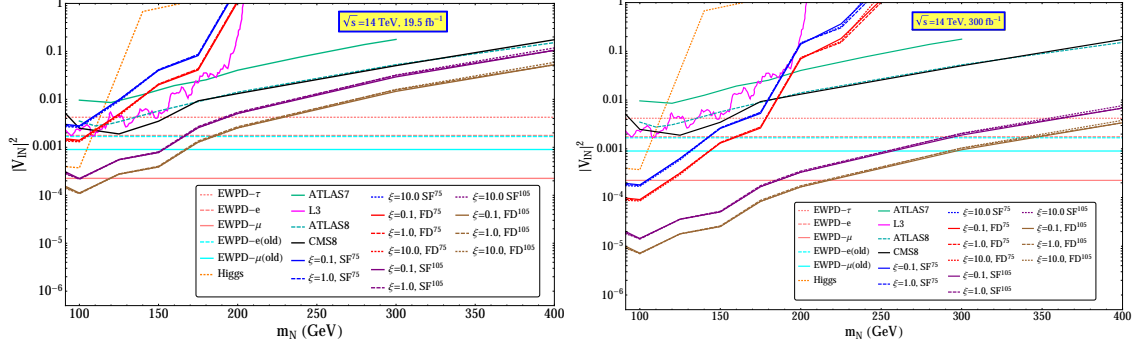


Figure 16. The prospective upper bounds on the light-heavy neutrino mixing angles $|V_{\ell N}|^2$ as a function of the heavy pseudo-Dirac neutrino mass m_N at 14 TeV LHC with 19.5 fb^{-1} (left panel) and 300 fb^{-1} (right panel) luminosities, derived from the CMS trilepton data at $\sqrt{s} = 8 \text{ TeV}$ LHC for 19.5 fb^{-1} luminosity [114] at 95 % CL. We have considered the scale dependent NLO case ($\xi = 0.1, 1.0, 10.0$) for the trilepton plus missing energy final state. Some relevant existing upper limits (all at 95% CL) are also shown for comparison: (i) from a χ^2 -fit to the LHC Higgs data [101] (Higgs), (ii) from a direct search at LEP [102](L3), valid only for the electron flavor, (iii) ATLAS limits from $\sqrt{s} = 7 \text{ TeV}$ LHC data [123] (ATLAS7) and $\sqrt{s} = 8 \text{ TeV}$ LHC data [100] (ATLAS8), valid for a heavy Majorana neutrino of the muon flavor, (iv) CMS limits from $\sqrt{s} = 8 \text{ TeV}$ LHC data [103] (CMS8), for a heavy Majorana neutrino of the muon flavor and (v) indirect limits from the global fit to the electroweak precision data (EWPD) from [104–106] for electron (cyan, EWPD-e(old)) and muon (cyan, EWPD- μ (old)) flavors (new values can be found from [107]), for tau (dotted, EWPD- τ) electron (solid, EWPD- e) and muon (dashed, EWPD- μ) flavors). Here SF^{75} and FD^{75} are the single flavor and flavor diagonal cases below the Z -pole whereas SF^{105} and FD^{105} are the same above the Z -pole.

cuts we compare them with the observed number of events at the 19.5 fb^{-1} luminosity [114]. For the selection criteria listed above, the CMS experiment observed:

- (a) 10 events with the SM background expectation of 11 ± 3.8 events for $m_{\ell^+\ell^-} < 75 \text{ GeV}$.
- (b) 4 events with the SM background expectation of 5.0 ± 1.6 events for $m_{\ell^+\ell^-} > 105 \text{ GeV}$.

In case (a) we have an upper limit of 2.8 signal events, while in case (b) leads to an upper limit of 0.6 signal events.

Using these limits, we can set an upper bound on $|V_{\ell N}|^2$ for a given value of m_N for the scale dependent NLO case. In Fig. 14 we plot our results of the prospective upper bounds for the SF and FD cases for the scale dependent NLO case at the 14 TeV. In [23] different H_T and E_T^{miss} regions are considered to calculate the upper bounds on the mixing angle which has been improved in [24] for the LO processes.

In this work we have considered a different region for H_T and E_T^{miss} to evaluate the upper bounds on the mixing angles which has not been tested before. In this new region we can put the prospective upper bounds on the mixing angle for the 14 TeV LHC for $m_N = 91.2 - 400$ GeV for the scale dependent NLO processes. We notice that for the trilepton case for the NLO processes at 14 TeV the scale dependent prospective bounds on mixing angle well coincide with each other. An estimation at the 100 TeV collider for the same study can make a legitimate improvement by approximately one order of magnitude or more and this will be tested in future. A prospective search reach for the 300 fb^{-1} luminosity at 14 TeV LHC is also given in Fig. 16 for which we can get up to order one improvement in the upper bounds of the mixing angles.

6 Conclusion

In this paper we have discussed the generation of the SM neutrino mass through the type-I and inverse seesaw mechanisms which involve the Majorana and the pseudo-Dirac heavy neutrinos respectively. Such heavy neutrinos, residing in the electroweak scale, can be produced at LHC and proposed 100 TeV hadron collider through a large mixing angle with the SM light neutrinos. To produce such heavy neutrinos at such high energy hadronic colliders it is important to discuss the scale dependent production cross-sections and distributions at the LO and also at the NLO QCD.

We have studied two different channels for the heavy neutrino production; one is the W mediated for the associated production of lepton and the other one is the Z mediated process with associated light neutrino. We have demonstrated that the heavy neutrino production cross-sections at the next-to-leading order QCD accuracy are quite stable against the scale variations, where as leading order estimated can change substantially. We also exhibit the scale dependance in different differential distributions related with the leptons and correlations between them.

We have obtained the prospective scale dependent search reach at the 14 TeV LHC and as well as at the 100 TeV collider for the Majorana heavy neutrino through the same sign dilepton plus dijet final state. Using the pseudo-Dirac heavy neutrinos we have studied the trilepton plus missing energy final state with jets and obtained the prospective search reach at the 14 TeV. A collider with a higher energy can probe the mixing angle more precisely improving the 14 TeV result up to an order of magnitude or more.

Acknowledgments

We thank Oliver Mattelaer and Valentin Hirshi for useful discussions and fixing bugs on `Madgraph5_aMC@NLO` when we were implementing the SM singlet heavy neutrinos in the MadGraph. AD would like to thank UC Davis and the organizers of Pre-SUSY 2015 and SUSY 2015 where a part of the work had been continued. Authors also thank V. Ravindran for useful discussions.

References

- [1] **CMS** Collaboration, S. Chatrchyan et al., *Observation of a new boson at a mass of 125 GeV with the CMS experiment at the LHC*, Phys.Lett. **B716** (2012) 30–61,
- [2] **ATLAS** Collaboration, G. Aad et al., *Observation of a new particle in the search for the Standard Model Higgs boson with the ATLAS detector at the LHC*, Phys.Lett. **B716** (2012) 1–29.
- [3] J. Beringer et. al. [Particle Data Group Collaboration], Phys. Rev. D 86, 010001 (2012).
- [4] K. Abe et. al. [T2K Collaboration] Phys. Rev. Lett. 107, 041801 (2011).
- [5] P. Adamson et al. [MINOS Collaboration], Phys. Rev. Lett. 107, 181802 (2011).
- [6] Y. Abe et al. [DOUBLE-CHOOZ Collaboration], Phys. Rev. Lett. 108, 131801 (2012).
- [7] F. P. An et al. [DAYA-BAY Collaboration], Phys. Rev. Lett. 108, 171803 (2012).
- [8] J. K. Ahn et al. [RENO Collaboration], Phys. Rev. Lett. 108, 191802 (2012).
- [9] T. Yanagida, “Horizontal Symmetry and Masses of Neutrinos,” Prog. Theor. Phys. **64**, 1103 (1980).
- [10] P. Minkowski, “ $\mu \rightarrow e\gamma$ at a Rate of One Out of 10^9 Muon Decays?,” Phys. Lett. B **67**, 421 (1977).
- [11] T. Yanagida, in Proceedings of the Workshop on the Unified Theory and the Baryon Number in the Universe (O. Sawada and A. Sugamoto, eds.), KEK, Tsukuba, Japan, 1979, p. 95;
- [12] M. Gell-Mann, P. Ramond, and R. Slansky, Supergravity (P. van Nieuwenhuizen et al. eds.), North Holland, Amsterdam, 1979, p. 315.
- [13] S. L. Glashow, The future of elementary particle physics, in Proceedings of the 1979 Cargèse Summer Institute on Quarks and Leptons (M. Levy et al. eds.), Plenum Press, New York, 1980, p. 687;
- [14] R. N. Mohapatra and G. Senjanovic, “Neutrino Mass and Spontaneous Parity Violation,” Phys. Rev. Lett. **44**, 912 (1980).
- [15] J. Schechter and J. W. F. Valle, “Neutrino Masses in $SU(2) \times U(1)$ Theories,” Phys. Rev. D **22**, 2227 (1980).

- [16] S. Weinberg , “Baryon and Lepton Nonconserving Processes,” Phys. Rev. Lett. **43**, 1566 (1979).
- [17] W. Y. Keung and G. Senjanovic, “Majorana Neutrinos and the Production of the Right-handed Charged Gauge Boson,” Phys. Rev. Lett. **50**, 1427 (1983).
doi:10.1103/PhysRevLett.50.1427
- [18] A. Datta, M. Guchait and D. P. Roy, “Prospect of heavy right-handed neutrino search at SSC / CERN LHC energies,” Phys. Rev. D **47**, 961 (1993)
doi:10.1103/PhysRevD.47.961 [hep-ph/9208228].
- [19] A. Datta, M. Guchait and A. Pilaftsis, “Probing lepton number violation via majorana neutrinos at hadron supercolliders,” Phys. Rev. D **50**, 3195 (1994)
doi:10.1103/PhysRevD.50.3195 [hep-ph/9311257].
- [20] J. A. Aguilar-Saavedra, “Heavy lepton pair production at LHC: Model discrimination with multi-lepton signals,” Nucl. Phys. B **828**, 289 (2010)
doi:10.1016/j.nuclphysb.2009.11.021 [arXiv:0905.2221 [hep-ph]].
- [21] C. Y. Chen and P. S. B. Dev, “Multi-Lepton Collider Signatures of Heavy Dirac and Majorana Neutrinos,” Phys. Rev. D **85**, 093018 (2012)
doi:10.1103/PhysRevD.85.093018 [arXiv:1112.6419 [hep-ph]].
- [22] A. Das and N. Okada, “Inverse seesaw neutrino signatures at the LHC and ILC,” Phys. Rev. D **88**, 113001 (2013) doi:10.1103/PhysRevD.88.113001 [arXiv:1207.3734 [hep-ph]].
- [23] A. Das, P. S. Bhupal Dev and N. Okada, “Direct bounds on electroweak scale pseudo-Dirac neutrinos from $\sqrt{s} = 8$ TeV LHC data,” Phys. Lett. B **735**, 364 (2014)
doi:10.1016/j.physletb.2014.06.058 [arXiv:1405.0177 [hep-ph]].
- [24] A. Das and N. Okada, “Improved bounds on the heavy neutrino productions at the LHC,” Phys. Rev. D **93**, no. 3, 033003 (2016) doi:10.1103/PhysRevD.93.033003 [arXiv:1510.04790 [hep-ph]].
- [25] P. S. Bhupal Dev and R. N. Mohapatra, “Unified explanation of the $eejj$, diboson and dijet resonances at the LHC,” Phys. Rev. Lett. **115**, no. 18, 181803 (2015)
doi:10.1103/PhysRevLett.115.181803 [arXiv:1508.02277 [hep-ph]].
- [26] A. Das, N. Nagata and N. Okada, “Testing the 2-TeV Resonance with Trileptons,” arXiv:1601.05079 [hep-ph].
- [27] J. Gluza, T. Jelinski and R. Szafron, “Lepton Number Violation and ‘Diracness’ of massive neutrinos composed of Majorana states,” arXiv:1604.01388 [hep-ph].
- [28] F. del Aguila and J. A. Aguilar-Saavedra, “Electroweak scale seesaw and heavy Dirac neutrino signals at LHC,” Phys. Lett. B **672**, 158 (2009)
doi:10.1016/j.physletb.2009.01.010 [arXiv:0809.2096 [hep-ph]].
- [29] F. del Aguila, J. A. Aguilar-Saavedra and R. Pittau, “Heavy neutrino signals at large hadron colliders,” JHEP **0710**, 047 (2007)
doi:10.1088/1126-6708/2007/10/047 [hep-ph/0703261].

- [30] J. A. Aguilar-Saavedra and F. R. Joaquim, “Measuring heavy neutrino couplings at the LHC,” *Phys. Rev. D* **86**, 073005 (2012) doi:10.1103/PhysRevD.86.073005 [arXiv:1207.4193 [hep-ph]].
- [31] B. P. Nayak and M. K. Parida, “Dilepton events with displaced vertices, double beta decay, and resonant leptogenesis with Type-II seesaw dominance, TeV scale Z' and heavy neutrinos,” arXiv:1509.06192 [hep-ph].
- [32] B. P. Nayak and M. K. Parida, “New mechanism for Type-II seesaw dominance in SO(10) with low-mass Z' , RH neutrinos, and verifiable LFV, LNV and proton decay,” *Eur. Phys. J. C* **75**, 183 (2015) doi:10.1140/epjc/s10052-015-3385-x [arXiv:1312.3185 [hep-ph]].
- [33] J. A. Aguilar-Saavedra, F. Deppisch, O. Kittel and J. W. F. Valle, “Flavour in heavy neutrino searches at the LHC,” *Phys. Rev. D* **85**, 091301 (2012) doi:10.1103/PhysRevD.85.091301 [arXiv:1203.5998 [hep-ph]].
- [34] R. Lal Awasthi and M. K. Parida, “Inverse Seesaw Mechanism in Nonsupersymmetric SO(10), Proton Lifetime, Nonunitarity Effects, and a Low-mass Z' Boson,” *Phys. Rev. D* **86**, 093004 (2012) doi:10.1103/PhysRevD.86.093004 [arXiv:1112.1826 [hep-ph]].
- [35] C. S. Fong, R. N. Mohapatra and I. Sung, “Majorana Neutrinos from Inverse Seesaw in Warped Extra Dimension,” *Phys. Lett. B* **704**, 171 (2011) doi:10.1016/j.physletb.2011.08.069 [arXiv:1107.4086 [hep-ph]].
- [36] A. G. Dias, C. A. de S. Pires and P. S. R. da Silva, “How the Inverse See-Saw Mechanism Can Reveal Itself Natural, Canonical and Independent of the Right-Handed Neutrino Mass,” *Phys. Rev. D* **84**, 053011 (2011) doi:10.1103/PhysRevD.84.053011 [arXiv:1107.0739 [hep-ph]].
- [37] A. Ibarra, E. Molinaro and S. T. Petcov, “Low Energy Signatures of the TeV Scale See-Saw Mechanism,” *Phys. Rev. D* **84**, 013005 (2011) doi:10.1103/PhysRevD.84.013005 [arXiv:1103.6217 [hep-ph]].
- [38] T. Saito *et al.*, “Extra dimensions and Seesaw Neutrinos at the International Linear Collider,” *Phys. Rev. D* **82**, 093004 (2010) [arXiv:1008.2257 [hep-ph]].
- [39] S. Banerjee, P. S. B. Dev, A. Ibarra, T. Mandal and M. Mitra, “Prospects of Heavy Neutrino Searches at Future Lepton Colliders,” arXiv:1503.05491 [hep-ph].
- [40] F. del Aguila, J. A. Aguilar-Saavedra and R. Pittau, “Heavy neutrino signals at large hadron colliders,” *JHEP* **0710**, 047 (2007) [hep-ph/0703261].
- [41] F. del Aguila and J. A. Aguilar-Saavedra, “Distinguishing seesaw models at LHC with multi-lepton signals,” *Nucl. Phys. B* **813**, 22 (2009) [arXiv:0808.2468 [hep-ph]].
- [42] B. Batell and M. McCullough, “Neutrino Masses from Neutral Top Partners,” *Phys. Rev. D* **92**, no. 7, 073018 (2015) doi:10.1103/PhysRevD.92.073018 [arXiv:1504.04016 [hep-ph]].

- [43] R. Leonardi, L. Alunni, F. Romeo, L. Fano and O. Panella, “Hunting for heavy composite Majorana neutrinos at the LHC,” arXiv:1510.07988 [hep-ph].
- [44] P. S. B. Dev, A. Pilaftsis, U. K. Yang, Phys. Rev. Lett. 112 (2014) 081801, arXiv:1308.2209 [hep-ph].
- [45] G. Bambhaniya, S. Khan, P. Konar and T. Mondal, “Constraints on a seesaw model leading to quasidegenerate neutrinos and signatures at the LHC,” Phys. Rev. D **91**, no. 9, 095007 (2015) [arXiv:1411.6866 [hep-ph]].
- [46] G. Bambhaniya, S. Goswami, S. Khan, P. Konar and T. Mondal, “Looking for hints of a reconstructible seesaw model at the Large Hadron Collider,” Phys. Rev. D **91**, 075007 (2015) [arXiv:1410.5687 [hep-ph]].
- [47] D. Alva, T. Han and R. Ruiz, “Heavy Majorana neutrinos from the $W\gamma$ fusion at hadron colliders”, J. High Energy Phys. **02** (2015) 072.
- [48] G. Dutta and A. S. Joshipura, “PseudoDirac neutrinos in seesaw model,” Phys. Rev. D **51**, 3838 (1995) doi:10.1103/PhysRevD.51.3838 [hep-ph/9405291].
- [49] N. Haba, S. Matsumoto and K. Yoshioka, “Observable Seesaw and its Collider Signatures,” Phys. Lett. B **677**, 291 (2009) doi:10.1016/j.physletb.2009.05.042 [arXiv:0901.4596 [hep-ph]].
- [50] S. Matsumoto, T. Nabeshima and K. Yoshioka, “Seesaw Neutrino Signals at the Large Hadron Collider,” JHEP **1006**, 058 (2010) doi:10.1007/JHEP06(2010)058 [arXiv:1004.3852 [hep-ph]].
- [51] S. Mondal, S. Biswas, P. Ghosh and S. Roy, “Exploring novel correlations in trilepton channels at the LHC for the minimal supersymmetric inverse seesaw model,” JHEP **1205**, 134 (2012) doi:10.1007/JHEP05(2012)134 [arXiv:1201.1556 [hep-ph]].
- [52] J. C. Helo, M. Hirsch and S. Kovalenko, “Heavy neutrino searches at the LHC with displaced vertices,” Phys. Rev. D **89**, 073005 (2014) doi:10.1103/PhysRevD.89.073005 [arXiv:1312.2900 [hep-ph]].
- [53] A. G. Hessler, A. Ibarra, E. Molinaro and S. Vogl, “Impact of the Higgs boson on the production of exotic particles at the LHC,” Phys. Rev. D **91**, no. 11, 115004 (2015) doi:10.1103/PhysRevD.91.115004 [arXiv:1408.0983 [hep-ph]].
- [54] F. F. Deppisch, P. S. Bhupal Dev and A. Pilaftsis, “Neutrinos and Collider Physics,” New J. Phys. **17**, no. 7, 075019 (2015) doi:10.1088/1367-2630/17/7/075019 [arXiv:1502.06541 [hep-ph]].
- [55] E. Arganda, M. J. Herrero, X. Marcano and C. Weiland, “Exotic $\mu\tau jj$ events from heavy ISS neutrinos at the LHC,” Phys. Lett. B **752**, 46 (2016) doi:10.1016/j.physletb.2015.11.013 [arXiv:1508.05074 [hep-ph]].
- [56] C. O. Dib and C. S. Kim, “Discovering sterile Neutrinos lighter than M_W at the LHC,” Phys. Rev. D **92**, no. 9, 093009 (2015) doi:10.1103/PhysRevD.92.093009 [arXiv:1509.05981 [hep-ph]].

- [57] C. Degrande, O. Mattelaer, R. Ruiz and J. Turner, “Fully-Automated Precision Predictions for Heavy Neutrino Production Mechanisms at Hadron Colliders,” arXiv:1602.06957 [hep-ph].
- [58] J. A. Casas and A. Ibarra, “Oscillating neutrinos and $\mu \rightarrow e \gamma$,” Nucl. Phys. B **618**, 171 (2001)[hep-ph/0103065].
- [59] R. N. Mohapatra, Phys. Rev. Lett. **56** (1986) 561.
- [60] R. N. Mohapatra and J. W. F. Valle, Phys. Rev. D **34**, 1642 (1986).
- [61] N. Arkani-Hamed, T. Han, M. Mangano and L. T. Wang, “Physics Opportunities of a 100 TeV Proton-Proton Collider,” arXiv:1511.06495 [hep-ph].
- [62] M. Magg and C. Wetterich, “Neutrino Mass Problem and Gauge Hierarchy,” Phys. Lett. B **94**, 61 (1980). doi:10.1016/0370-2693(80)90825-4
- [63] T. P. Cheng and L. F. Li, “Neutrino Masses, Mixings and Oscillations in $SU(2) \times U(1)$ Models of Electroweak Interactions,” Phys. Rev. D **22**, 2860 (1980). doi:10.1103/PhysRevD.22.2860.
- [64] G. Lazarides, Q. Shafi and C. Wetterich, “Proton Lifetime and Fermion Masses in an $SO(10)$ Model,” Nucl. Phys. B **181**, 287 (1981). doi:10.1016/0550-3213(81)90354-0
- [65] R. N. Mohapatra and G. Senjanovic, “Neutrino Masses and Mixings in Gauge Models with Spontaneous Parity Violation,” Phys. Rev. D **23**, 165 (1981). doi:10.1103/PhysRevD.23.165
- [66] A. Melfo, M. Nemevsek, F. Nesti, G. Senjanovic and Y. Zhang, “Type II Seesaw at LHC: The Roadmap,” Phys. Rev. D **85**, 055018 (2012), doi:10.1103/PhysRevD.85.055018.
- [67] E. J. Chun and P. Sharma, “Same-Sign Tetra-Leptons from Type II Seesaw,” JHEP **1208**, 162 (2012) doi:10.1007/JHEP08(2012)162 [arXiv:1206.6278 [hep-ph]].
- [68] E. J. Chun, H. M. Lee and P. Sharma, “Vacuum Stability, Perturbativity, EWPD and Higgs-to-diphoton rate in Type II Seesaw Models,” JHEP **1211**, 106 (2012) doi:10.1007/JHEP11(2012)106 [arXiv:1209.1303 [hep-ph]].
- [69] P. S. Bhupal Dev, D. K. Ghosh, N. Okada and I. Saha, “125 GeV Higgs Boson and the Type-II Seesaw Model,” JHEP **1303**, 150 (2013), [JHEP **1305**, 049 (2013)] doi:10.1007/JHEP03(2013)150, 10.1007/JHEP05(2013)049, [arXiv:1301.3453 [hep-ph]]
- [70] E. J. Chun and P. Sharma, “Search for a doubly-charged boson in four lepton final states in type II seesaw,” Phys. Lett. B **728**, 256 (2014) doi:10.1016/j.physletb.2013.11.056 [arXiv:1309.6888 [hep-ph]].
- [71] P. H. Gu, H. Zhang and S. Zhou, “A Minimal Type II Seesaw Model,” Phys. Rev. D **74**, 076002 (2006), doi:10.1103/PhysRevD.74.076002.
- [72] N. Haba, H. Ishida, N. Okada and Y. Yamaguchi, “Vacuum stability and naturalness in type-II seesaw,” arXiv:1601.05217 [hep-ph].

- [73] Z. L. Han, R. Ding and Y. Liao, “LHC Phenomenology of Type II Seesaw: Nondegenerate Case,” *Phys. Rev. D* **91**, 093006 (2015) doi:10.1103/PhysRevD.91.093006 [arXiv:1502.05242 [hep-ph]].
- [74] Z. L. Han, R. Ding and Y. Liao, “LHC phenomenology of the type II seesaw mechanism: Observability of neutral scalars in the nondegenerate case,” *Phys. Rev. D* **92**, no. 3, 033014 (2015) doi:10.1103/PhysRevD.92.033014 [arXiv:1506.08996 [hep-ph]].
- [75] R. Foot, H. Lew, X. G. He and G. C. Joshi, “Seesaw Neutrino Masses Induced by a Triplet of Leptons,” *Z. Phys. C* **44**, 441 (1989). doi:10.1007/BF01415558
- [76] R. Franceschini, T. Hambye and A. Strumia, “Type-III see-saw at LHC,” *Phys. Rev. D* **78**, 033002 (2008), doi:10.1103/PhysRevD.78.033002, [arXiv:0805.1613 [hep-ph]].
- [77] A. Abada, C. Biggio, F. Bonnet, M. B. Gavela and T. Hambye, “ $\mu \rightarrow e \gamma$ and $\tau \rightarrow \ell \gamma$ decays in the fermion triplet seesaw model,” *Phys. Rev. D* **78**, 033007 (2008), doi:10.1103/PhysRevD.78.033007, [arXiv:0803.0481 [hep-ph]].
- [78] J. A. Aguilar-Saavedra, P. M. Boavida and F. R. Joaquim, “Flavored searches for type-III seesaw mechanism at the LHC,” *Phys. Rev. D* **88**, 113008 (2013) doi:10.1103/PhysRevD.88.113008 [arXiv:1308.3226 [hep-ph]].
- [79] O. J. P. Eboli, J. Gonzalez-Fraile and M. C. Gonzalez-Garcia, “Neutrino Masses at LHC: Minimal Lepton Flavour Violation in Type-III See-saw,” *JHEP* **1112**, 009 (2011) doi:10.1007/JHEP12(2011)009 [arXiv:1108.0661 [hep-ph]].
- [80] Y. H. Ahn, C. S. Kim and S. Oh, “Recent Neutrino Data and Type III Seesaw with Discrete Symmetry,” *Phys. Rev. D* **86**, 013007 (2012) doi:10.1103/PhysRevD.86.013007 [arXiv:1103.0657 [hep-ph]].
- [81] C. Biggio and F. Bonnet, “Implementation of the Type III Seesaw Model in FeynRules/MadGraph and Prospects for Discovery with Early LHC Data,” *Eur. Phys. J. C* **72**, 1899 (2012), doi:10.1140/epjc/s10052-012-1899-z, [arXiv:1107.3463 [hep-ph]].
- [82] R. Franceschini, T. Hambye and A. Strumia, “Type-III see-saw at LHC,” *Phys. Rev. D* **78**, 033002 (2008), doi:10.1103/PhysRevD.78.033002, [arXiv:0805.1613 [hep-ph]].
- [83] R. Ruiz, “QCD Corrections to Pair Production of Type III Seesaw Leptons at Hadron Colliders,” *JHEP* **1512**, 165 (2015) doi:10.1007/JHEP12(2015)165 [arXiv:1509.05416 [hep-ph]].
- [84] K. S. Babu, S. Nandi and Z. Tavartkiladze, “New Mechanism for Neutrino Mass Generation and Triply Charged Higgs Bosons at the LHC,” *Phys. Rev. D* **80**, 071702 (2009), doi:10.1103/PhysRevD.80.071702, [arXiv:0905.2710 [hep-ph]].
- [85] G. Bambhaniya, J. Chakraborty, S. Goswami and P. Konar, “Generation of neutrino mass from new physics at TeV scale and multilepton signatures at the

- LHC,” Phys. Rev. D **88**, no. 7, 075006 (2013), doi:10.1103/PhysRevD.88.075006, [arXiv:1305.2795 [hep-ph]].
- [86] I. Gogoladze, N. Okada and Q. Shafi, “NMSSM and Seesaw Physics at LHC,” Phys. Lett. B **672**, 235 (2009) doi:10.1016/j.physletb.2008.12.068 [arXiv:0809.0703 [hep-ph]].
- [87] J. Alwall, M. Herquet, F. Maltoni, O. Mattelaer and T. Stelzer, “MadGraph 5 : Going Beyond,” JHEP **1106**, 128 (2011)[arXiv:1106.0522 [hep-ph]].
- [88] J. Alwall, M. Herquet, F. Maltoni, O. Mattelaer, T. Stelzer, J. High Energy Phys. 1106 (2011) 128, arXiv: 1106.0522 [hep-ph]
- [89] J. Alwall, R. Frederix, S. Frixione, V. Hirschi, F. Maltoni, O. Mattelaer, H.-S. Shao and T. Stelzer *et al.*, “The automated computation of tree-level and next-to-soft order differential cross-sections, and their matching to parton shower simulations,” J. High Energy Phys. **1407**, 079 (2014) [arXiv:1405.0301 [hep-ph]].
- [90] V. Hirschi *et. al* “Automation of oneloop QCD corrections,” JHEP **05** (2011) 044, [1103.0621].
- [91] R. Frederix, S. Frixione, F. Maltoni and T. Stelzr, “Automation of next-to-leading order computations in QCD: the FKS subtraction,” JHEP **10** (2009) 003, [0908.4272].
- [92] G. Ossola, C. G. Papadopoulos and R. Pittau, “Reducing full one-loop amplitudes to scalar integrals at the integrand level” , Nucl.Phys.**B763** (2007) 147-169, [hep-ph/0609007].
- [93] G. Ossola, C. G. Papadopoulos and R. Pittau, CutTools: A Program implementing the OPP reduction method to compute one-loop amplitudes,” JHEP **0803** (2008)042, [0711.3596].
- [94] S. Frixione, Z. Kunszt and A. Signer, ”Three-jet cross sections to next-to-leading order,” Nucl.Phys.**B467** (1996) 399-442, [hep-ph/9512328].
- [95] T. Sjostrand, S. Mrenna, P. Z. Skands, J. High Energy Phys. 0605 (2006) 026, arXiv: hep-ph/0603175.
- [96] M. Cacciari, G. P. Salam and G. Soyez, Eur. Phys. J. C **72**, 1896 (2012), [arXiv:1111.6097 [hep-ph]].
- [97] <https://bugs.launchpad.net/mg5amcnlo/+bug/1466242>
- [98] <https://answers.launchpad.net/mg5amcnlo/+question/281103>
- [99] <http://folk.uio.no/maikenp/pages/MadGraph/Manual-March-2007.pdf>
- [100] G. Aad *et al.* [ATLAS Collaboration], “Search for heavy Majorana neutrinos with the ATLAS detector in pp collisions at $\sqrt{s} = 8$ TeV,” JHEP **1507**, 162 (2015) doi:10.1007/JHEP07(2015)162 [arXiv:1506.06020 [hep-ex]].
- [101] P. S. Bhupal Dev, R. Franceschini and R. N. Mohapatra, “Bounds on TeV Seesaw

- Models from LHC Higgs Data,” *Phys. Rev. D* **86**, 093010 (2012)
doi:10.1103/PhysRevD.86.093010 [arXiv:1207.2756 [hep-ph]].
- [102] P. Achard *et al.* [L3 Collaboration], “Search for heavy isosinglet neutrino in e^+e^- annihilation at LEP,” *Phys. Lett. B* **517**, 67 (2001)
doi:10.1016/S0370-2693(01)00993-5 [hep-ex/0107014].
- [103] V. Khachatryan *et al.* [CMS Collaboration], “Search for heavy Majorana neutrinos in $\mu^\pm\mu^\pm +$ jets events in proton-proton collisions at $\sqrt{s} = 8$ TeV,” *Phys. Lett. B* **748**, 144 (2015) doi:10.1016/j.physletb.2015.06.070 [arXiv:1501.05566 [hep-ex]].
- [104] J. de Blas, “Electroweak limits on physics beyond the Standard Model,” *EPJ Web Conf.* **60**, 19008 (2013) doi:10.1051/epjconf/20136019008 [arXiv:1307.6173 [hep-ph]].
- [105] F. del Aguila, J. de Blas and M. Perez-Victoria, “Effects of new leptons in Electroweak Precision Data,” *Phys. Rev. D* **78**, 013010 (2008)
doi:10.1103/PhysRevD.78.013010 [arXiv:0803.4008 [hep-ph]].
- [106] E. Akhmedov, A. Kartavtsev, M. Lindner, L. Michaels and J. Smirnov, “Improving Electro-Weak Fits with TeV-scale Sterile Neutrinos,” *JHEP* **1305**, 081 (2013)
doi:10.1007/JHEP05(2013)081 [arXiv:1302.1872 [hep-ph]].
- [107] S. Antusch, E. Cazzato and O. Fischer, “Higgs production from sterile neutrinos at future lepton colliders,” arXiv:1512.06035 [hep-ph].
- [108] S. Antusch and O. Fischer, “Non-unitarity of the leptonic mixing matrix: Present bounds and future sensitivities,” *JHEP* **1410**, 094 (2014)
doi:10.1007/JHEP10(2014)094 [arXiv:1407.6607 [hep-ph]].
- [109] L. Basso, O. Fischer and J. J. van der Bij, “Precision tests of unitarity in leptonic mixing,” *Europhys. Lett.* **105**, no. 1, 11001 (2014)
doi:10.1209/0295-5075/105/11001 [arXiv:1310.2057 [hep-ph]].
- [110] S. Antusch and O. Fischer, “Testing sterile neutrino extensions of the Standard Model at the Circular Electron Positron Collider,” *Int. J. Mod. Phys. A* **30**, no. 23, 1544004 (2015). doi:10.1142/S0217751X15440042
- [111] S. Antusch and O. Fischer, “Testing sterile neutrino extensions of the Standard Model at future lepton colliders,” *JHEP* **1505**, 053 (2015)
doi:10.1007/JHEP05(2015)053 [arXiv:1502.05915 [hep-ph]].
- [112] J. Pumplin, D. R. Stump, J. Huston, H. L. Lai, P. M. Nadolsky and W. K. Tung, “New generation of parton distributions with uncertainties from global QCD analysis,” *JHEP* **0207**, 012 (2002) doi:10.1088/1126-6708/2002/07/012 [hep-ph/0201195].
- [113] J. de Favereau *et al.* [DELPHES 3 Collaboration], “DELPHES 3, A modular framework for fast simulation of a generic collider experiment,” *JHEP* **1402**, 057 (2014) doi:10.1007/JHEP02(2014)057 [arXiv:1307.6346 [hep-ex]].

- [114] S. Chatrchyan *et al.* [CMS Collaboration], “Search for anomalous production of events with three or more leptons in pp collisions at $\sqrt{s} = 8$ TeV,” *Phys. Rev. D* **90**, 032006 (2014) doi:10.1103/PhysRevD.90.032006 [arXiv:1404.5801 [hep-ex]].
- [115] Z. Kang, P. Ko and J. Li, “New Avenues to Heavy Right-handed Neutrinos with Pair Production at Hadronic Colliders,” arXiv:1512.08373 [hep-ph].
- [116] W. Abdallah, J. Fiaschi, S. Khalil and S. Moretti, “Z'-induced invisible right-handed sneutrino decays at the LHC,” *Phys. Rev. D* **92**, 055029 (2015) doi:10.1103/PhysRevD.92.055029
- [117] W. Abdallah, J. Fiaschi, S. Khalil and S. Moretti, “Mono-jet, -photon and -Z signals of a supersymmetric (B - L) model at the Large Hadron Collider,” *JHEP* **1602**, 157 (2016) doi:10.1007/JHEP02(2016)157 [arXiv:1510.06475 [hep-ph]].
- [118] S. Khalil and S. Moretti, “The $B - L$ Supersymmetric Standard Model with Inverse Seesaw at the Large Hadron Collider,” arXiv:1503.08162 [hep-ph].
- [119] A. Elsayed, S. Khalil and S. Moretti, “Higgs Mass Corrections in the SUSY B-L Model with Inverse Seesaw,” *Phys. Lett. B* **715**, 208 (2012) doi:10.1016/j.physletb.2012.07.066 [arXiv:1106.2130 [hep-ph]].
- [120] M. Abbas, S. Khalil, A. Rashed and A. Sil, “Neutrino masses and deviation from tribimaximal mixing in $\Delta(27)$ model with inverse seesaw mechanism,” *Phys. Rev. D* **93**, no. 1, 013018 (2016) doi:10.1103/PhysRevD.93.013018 [arXiv:1508.03727 [hep-ph]].
- [121] S. Khalil and C. S. Un, “Muon Anomalous Magnetic Moment in SUSY B-L Model with Inverse Seesaw,” arXiv:1509.05391 [hep-ph].
- [122] K. Huitu, S. Khalil, H. Okada and S. K. Rai, “Signatures for right-handed neutrinos at the Large Hadron Collider,” *Phys. Rev. Lett.* **101**, 181802 (2008) doi:10.1103/PhysRevLett.101.181802 [arXiv:0803.2799 [hep-ph]].
- [123] [ATLAS Collaboration], “Search for Majorana neutrino production in pp collisions at $\sqrt{s} = 7$ TeV in dimuon final states with the ATLAS detector,” ATLAS-CONF-2012-139; S. Chatrchyan *et al.* [CMS Collaboration], “Search for heavy Majorana neutrinos in $\mu^\pm\mu^\pm + \text{jets}$ and $e^\pm e^\pm + \text{jets}$ events in pp collisions at $\sqrt{s} = 7$ TeV,” *Phys. Lett. B* **717**, 109 (2012) doi:10.1016/j.physletb.2012.09.012 [arXiv:1207.6079 [hep-ex]].